RADIAL TEMPERATURE DERIVED FROM PROBE CONDUCTANCE MEASUREMENTS IN A RECOVERING SPARK CHANNEL

by

REGINALD MONTGOMERY CLEMENTS

B.A.Sc., University of British Columbia, 1963

A THESIS SUBMITTED IN PARTIAL FULFILMENT OF

THE REQUIREMENTS FOR THE DEGREE OF

MASTER OF APPLIED SCIENCE

in the Department

of

PHYSICS

We accept this thesis as conforming to the

required standard

THE UNIVERSITY OF BRITISH COLUMBIA

August, 1964

In presenting this thesis in partial fulfilment of the requirements for an advanced degree at the University of British Columbia, I agree that the Library shall make it freely available for reference and study. I further agree that permission for extensive copying of this thesis for scholarly purposes may be granted by the Head of my Department or by his representatives. It is understood that copying or publication of this thesis for financial gain shall not be allowed without my written permission.

Department of Physics

The University of British Columbia,
Vancouver 8, Canada

Date August 15, 1964.

ABSTRACT

The conductance of a small electric probe has been determined for radial distances (2 - 15 cm) from a recovering spark gap as a function of time after discharge initiation. The times investigated were from 0.2 to 15 ms and the gas pressure was varied from 22 mmHg down to 0.1 mmHg. The voltage applied to the probes was a sawtooth pulse which rose to about 80 volts in 10 μs.

It is shown theoretically that the probe conductance should be proportional to the three-halves power of the gas temperature. From a known value of the temperature, deduced from recovery measurements, and the known probe conductance the constant of proportionality was deduced. Hence it was possible to determine the temperature from the probe conductance.

The probe conductance measurements show that at 200 mmHg pressure the spark channel is only 2 cm in radius and that there is no detectable ionization left 2 ms after the discharge. As the gas pressure decreases the spark channel increases in size and takes longer to deionize, until at 1 mmHg pressure the channel fills the whole spark chamber (spark channel radius is 15 cm) and requires almost 15 ms to deionize. At 1 mmHg gas pressure there is a radial temperature gradient, while at 0.1 mmHg pressure the gas everywhere in the channel recovers at the

same rate.

In this experiment it is theoretically predicted that volume recombination should be the dominant recovery method and this is experimentally verified.

ACKNOWLEDGEMENT

I would like to offer my sincere thanks to my supervisor, Dr. R.J. Churchill, for the help which he gave me while I was setting up and performing this experiment, and also for the help which he gave when I was analyzing the results and writing up the thesis, even though he was no longer associated with this University.

I also gratefully acknowledge the work of Dr. R.A. Nodwell in reading the thesis manuscript and offering his valuable suggestions.

I would also like to thank Mr. John Turner who built and maintained the electronic equipment used in this experiment and offered valuable technical advice.

TABLE OF CONTENTS

LIST OF ILLUSTRATIONS

INTRODUCTION

The spark gap is extensively employed as an electrical switch in various pulsed plasma generation devices. It is also useful as a source of high temperature plasma. Fischer (1957) reports that, using an especially developed low inductance capacitor, he obtained temperatures of about 250,000 ^{o}K in a helium plasma at atmospheric pressure. The characteristics of the recovering plasma formed from the passage of the spark, are of interest to engineers, not only in the design of circuit breakers but also in the possible use of spark gaps as recurrent switches in some thermonuclear devices. From a more fundamental point of view, a knowledge of the properties, especially particle densities and temperatures, would lead to a better understanding of the basic processes responsible for the decay of the plasma.

Due to the usefulness of spark gaps as switches, the reignition voltage characteristics for surge currents as high as 235 kA have been experimentally determined (23 kA - McCann and Clark, 1943; 235 kA - Churchill, 1960; 40 kA - Chan, 1963). The later two investigators measured the reignition voltage as a function of the radial distance from the main spark gap as well as a function of the time after spark initiation. By assuming that the spark reignited in accordance to Paschen's law, the gas temperature was derived. This assumption, however,

is only true during the later part of the recovery, since during this period there is little or no ionization present, i.e. reignition voltages are lowered mainly due to the decreased gas density. Poole, Parker, and Churchill (1963) confirmed the temperatures derived from reignition measurements by using a plane shock wave to probe the recovering gas. By measuring the velocity of this shock with Schlieren techniques the radial temperature distribution of the spark channel was determined. This technique has also been used, under different experimental conditions, by Allen, Edels, and Whittaker (1961). Some time-resolved spectroscopic investigations of recovering spark channels have also been made. Vanyukov, et al, (1959) made time resolved measurements in a system where the energy stored in the capacitor bank was quite small (less than 2 joules) and the gas pressure was equal to or greater than atmospheric pressure. Craggs (1963) obtained oscillographic traces of line intensities for a number of spectral lines of argon and helium. The pressures investigated were from 760 to 50 mm.Hg but the spark current was much lower than that employed in this experiment. Both Craggs and Vanyukov found that the spark chanel was luminous only for a few micro-seconds although the period of luminoscity increased when gas pressure decreased.

Up to the present time it does not appear that temperatures have been deduced on the basis of electric probe measurements. In these measurements the probes are immersed in the plasma and

a voltage applied between the probes. This voltage is small enough so that spark breakdown between the probes does not occur and the current flow between the probes is dependent on the plasma conductivity. In the present investigation it was originally planned to use the classical double floating probe of Johnson and Malter (1950) to determine the electron temperature. However, due to difficulties in isolating the probes from ground while still ensuring that the observed current was the actual current flowing in the probe circuit, this approach was abandoned and probe impedence measurements were made. From these measurements it was possible to deduce the temperature. For a spark taking place in a relatively high pressure gas equilibrium between the electrons, ions, and the neutral gas particles is rapidly established so that the electron (T_e), ion (T_i), and gas (T_g) temperatures all have the same value which is referred to as the temperature (T) i.e. $T_e \approx T_i \approx T_g \approx T$. This point is considered in some detail in section 1.1.

Electric probes have certain advantages over the above methods of temperature determination. Compared to the spectroscopic and shock wave measurements the probes have a high degree of spatial resolution, and unlike the reignition measurements the temperature can still be determined when there is appreciable ionization. As these probe measurements depend on the electrical conductivity of the gas, low gas pressures (below 200 mmHg) were used in order that a reasonable current

(greater than 1 μamp) flowed between the probes. Unfortunately, in all works previously referred to, the gas pressures have been greater than those used in this experiment so that direct comparisons are difficult to make.

The next main section of this thesis discusses, theoretically, the processes by which the spark channel recovers, the formation of ion sheaths, and the temperature from probe conductance measurements. Following this, the apparatus used in the experiment and the methods by which the measurements were made are presented. Samples of the data taken are reproduced and discussed. In Chapter 4 the temperature is determined from the probe conductance measurements. These results are discussed in Chapter 5 and the limitations on them pointed out. It is concluded in Chapter 6 that probe measurements yield a great deal of data and, even using the relatively simple analysis proposed here, information about temperatures of the recovering plasma can be obtained.

CHAPTER 1: THEORY OF SPARK GAP RECOVERY AND THE THEORY OF PROBES

In this section a brief survey of the mechanisms which effect the recovery of the spark gap is given. As the mathematics yield equations which cannot be solved without making approximations when there is a combination of mechanisms influencing the recovery, each mechanism will be dealt with singly, as if it were the only mechanism responsible for the recovery. Probe theory and gas conductivity are discussed in the second section and the relationships necessary to calculate the temperature from the probe impedence are derived.

1.1 RECOVERY AND DEIONIZATION

Upon the passage of a high current through a spark gap, the test gas becomes highly ionized. The degree of ionization is probably about 100 per cent, as Vayukov, et al, (1959) have observed spectra of doubly ionized atoms in a low energy spark.

Craig and Craggs (1953) have estimated that thermal equilibrium is rapidly established, but they considered only cases of high gas pressure. If times of interest are much greater than the characteristic relaxation times for electron-electron (τ_1), ion-ion (τ_2), and electron-ion (τ_3)

collisions, then the plasma can be assumed to be in thermal equilibrium. The ion temperature will be essentially equal to the neutral gas temperature, as both the ion and the atom have essentially the same mass. From Delcroix (1960), and Spitzer (1956), one finds that:

$$\tau_1 \approx \frac{3.8 \times 10^5 \, T^{3/2}}{n_e \ln \Lambda} \quad \text{(sec.)}$$

$$\tau_2 \approx \left(\frac{M}{m}\right)^{1/2} \tau_1 \quad \text{(sec.)}$$

$$\tau_3 \approx \frac{M}{m} \tau_1 \quad \text{(sec.)}$$

where: M = ion mass (kg)

m = electron mass (kg)

T = temperature (^oK)

n_e = electron concentration (electrons meter^{-3})

$$\Lambda = \frac{\lambda_D}{b_o}$$

Here: λ_D = Debye shielding distance = $\sqrt{\frac{\epsilon_o kT}{q_e^2 n_e}}$ (meter)

b_o = impact parameter for 90° deflection

$$= \frac{q_e^2}{12 \epsilon_o kT} \quad \text{(meter)}$$

where: ϵ_o = permitivity of vacuum (farad meter^{-1})

k = Boltzmann's constant (joules $^oK^{-1}$)

q_e = electron charge (coulombs)

Table I shows order of magnitude values of τ_1, τ_2, and τ_3

assuming 100 per cent ionization and a temperature of 10^5 °K. For the value of M, the mass of the nitrogen ion is used and the values of $\ln\Lambda$ are from Spitzer (1956, table 5.2).

TABLE I RELAXATION TIMES FOR ELECTRON-ELECTRON, ION-ION, AND ELECTRON-ION COLLISIONS

Pressure (mmHg)	n meter^{-3}	T (°K)	$\ln\Lambda$ approx.	τ_1 (sec.)	τ_2 (sec.)	τ_3 (sec.)
760	3×10^{25}	10^5	5	10^{-13}	10^{-11}	10^{-9}
10	3×10^{23}	10^5	7	10^{-12}	10^{-9}	10^{-7}
1	3×10^{22}	10^5	8	10^{-11}	10^{-8}	10^{-6}
0.1	3×10^{21}	10^5	9	10^{-10}	10^{-7}	10^{-5}

From this table one sees that at atmospheric pressure thermal equilibrium is established very rapidly but at lower pressures for certain types of measurement, the assumption of thermal equilibrium may not be valid. In this experiment the channel was allowed to recover freely for at least 200 μs before any measurements were made, and by this time, even for low pressures $T_e \approx T_i \approx T_g$.

The hot, highly ionized gas recovers to a neutral gas at room temperature by a number of processes. During the actual discharge there is a large current and hence an associated magnetic field. It is then possible that cyclotron radiation from electrons could be an important energy loss mechanism.

This mechanism is probably not very important as the current pulse, and hence the associated magnetic field is of very short duration (about 10 μs). Also detailed consideration of the power radiated per unit solid angle (see for example Rose and Clark, 1961, section 11.3) shows that the cyclotron radiation is only important for relativistic electrons.

Another possible energy loss mechanism is bremsstrahlung radiation produced by electron acceleration in the field of an ion. By assuming that the electrons have a Maxwell-Boltzmann distribution, the power density radiated by all electrons (see for example Rose and Clark, section 11.2) is proportional to the product of the electron and ion densities, $T_e^{\frac{1}{2}}$, and Z^2 where T_e is the electron temperature and Z the ionic charge number. During the spark discharge a considerable amount of electrode material boils off, which gives rise to high Z impurities. In practice, however, bremsstrahlung radiation losses are not important, even in the presence of high Z impurities, for temperatures less than thermonuclear temperatures. In the present experiment maximum temperatures are well below these values.

The preceding two energy loss mechanisms do not decrease the electron density, i.e. little, or no, deionization takes place. In this experiment deionization occurs in two ways. First, the electron will recombine with positive ions. This

process, when it occurs remote from the walls, is called volume recombination or simply recombination. Secondly, the electrons will diffuse to the walls, and because of the presence of a third body, will disappear by wall recombination.

Recombination between positive ions and electrons may take place in a variety of ways. The two most important are direct recombination of an ion and an electron in which the excess electron energy is given off as radiation, and three-body recombination. In three-body recombination the electron approaches an ion which is in the neighbourhood of a third body and the electron gives up its excess energy to this third body before combining with the ion. This mechanism, although occurring, is not very probable, except near the walls of the spark chamber.

If the plasma is assumed to be approximately neutral ($n_+ \approx n_e \approx n$) then the effect of recombination on particle concentration can be described by:

$$\frac{dn}{dt} = -\alpha n_+ n_e = -\alpha n^2 \qquad \ldots 1$$

where: t = time (sec.)

n_+ = ion concentration (ions meter^{-3})

n_e = electron concentration (electrons meter^{-3})

α = recombination coefficient (meter^3 sec.$^{-1}$)

From equation 1 one sees that the relative loss rate $\frac{1}{n}\frac{dn}{dt}$

is proportional to the electron density. Hence volume recombination would tend to make the density uniform since the relative loss rate is greater in regions of higher concentration. Since the rate of electron loss by volume recombination is proportional to n^2, volume recombination will predominate over diffusion losses when there is a high degree of ionization present or at high pressures. In this experiment where relatively high pressures are used and the initial degree of ionization is very high, volume recombination is the dominant deionization mechanism, at least in the early part of the recovery period. The radiation emitted by the direct recombination of an ion and a free electron accounts for the continuum radiation of the spark channel.

If the Debye shielding distance is much smaller than the dimensions of the vessel, then the charged particles will diffuse by ambipolar diffusion. For the densities and temperatures in this experiment the foregoing criterion holds. Recombination takes place readily at the walls since the atoms or molecules of the wall materials are available to act as a third body and take up the liberated energy. This results in a density gradient away from the walls. Because of the difference in masses, the electrons diffuse more rapidly than the ions. This leads to charge separation which results in a space charge field. This field retards the diffusion of the

electrons and increases the diffusion of the ions. Hence one would expect that electrons and ions diffuce at the same rate. Assuming that this is true, that the plasma is quasi neutral, that both electrons and ions have a Maxwell-Boltzmann distribution, that the plasma is isothermal and composed of one type of ion. then the diffusion is described by:

$$\bar{\Gamma} = -D_a \nabla n \qquad \ldots 2$$

where: $\bar{\Gamma}$ = particle flux (number meter^{-2} sec.$^{-1}$)

D_a = ambipolar diffucion coefficient

$$= 2\mu_+ \frac{kT}{q_e} \quad (\text{meter}^3 \text{ sec.}^{-1}) \qquad \ldots 3$$

and: μ_+ = positive ion mobility

= velocity/unit field (volts sec.$^{-1}$).

Substituting equation 2 into the continuity equation yields a description of the time and spatial variation of density:

$$\frac{\partial n}{\partial t} = D_a \nabla^2 n \qquad \ldots 4$$

From 4 it is seen that a large value of D_a will make diffusion the predominant recovery mechanism. The conditions for this, as the mobility increases as the pressure decreases, are low pressure and high temperature.

In this experiment the early part of the recovery is controlled primarily by recombination, especially at high pressures, but at lower pressures diffusion should become more

important. When both these effects are taking place simultaneously it is, however, very difficult to say which, if either, is predominant.

Competing against the processes of deionization is the process of thermal ionization. This term applies to ionization produced by molecular or electron collisions and by radiation. Especially at high pressures, where the mean free path is very short, this may be an important factor in the determination of the over-all recovery, and it is the prime source of ionization during the recovery period.

The latter part of the recovery, where ionization is low, is controlled primarily by gas convection and thermal conduction. Here the hot gas transfers its energy to the cool walls and cool electrodes. The electrode tips may be hotter than the gas is, in which case the process will be reversed in this region of space.

The gas is fully recovered when it returns to its unionized state at ambient temperature.

1.2 PROBE AND CONDUCTIVITY THEORY

As was shown in Section 1.1, for the conditions of this experiment, the plasma is in thermal equilibrium. Even under these circumstances the electron velocity will be much greater

than the ion velocity, due to the smaller mass of the electron, and many more electrons, per unit time, will strike the walls of the chamber than ions. These electrons build up a negative surface charge on the walls. This surface charge repels those electrons near the walls and results in a small region next to the wall where there is an excess of positive ions -- the positive ion space-charge sheath. The thickness of this sheath is approximately the Debye shielding distance. This point of view yields a physical interpretation of the Debye distance, as that distance over which charge neutrality is not necessarily maintained. The preceding arguments are not then in contradiction to the assumption of plasma neutrality, over large distances from the electrodes compared with the Debye distance, which was made in the discussion on ambipolar diffusion.

The result of the positive ion sheath is that the plasma potential will be slightly above the floating wall potential. It is assumed that the sheath potential, or in general any external potential applied to the plasma, has little or no effect on the ion motion. This assumption is due to the fact that the electron mobility is much greater than the ion mobility On the basis of the foregoing arguments, the expected potentials near to a wall of the spark chamber are shown in Figure 1.1.

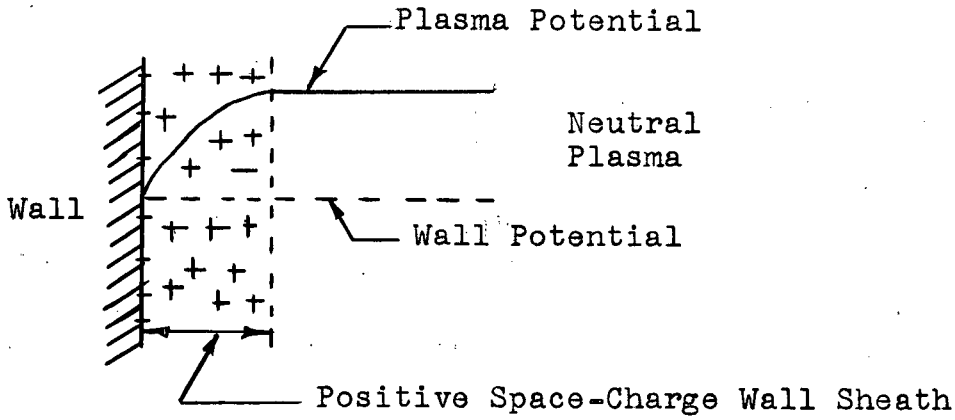

FIGURE 1.1 POTENTIAL DIAGRAM FOR PLASMA NEAR A WALL

Two probes, of equal area and with no voltage between them, when inserted in the plasma, will be also surrounded by a positive ion sheath in the same way that the walls are. Figure 1.2 shows a schematic diagram of the double probe circuit where one probe is grounded.

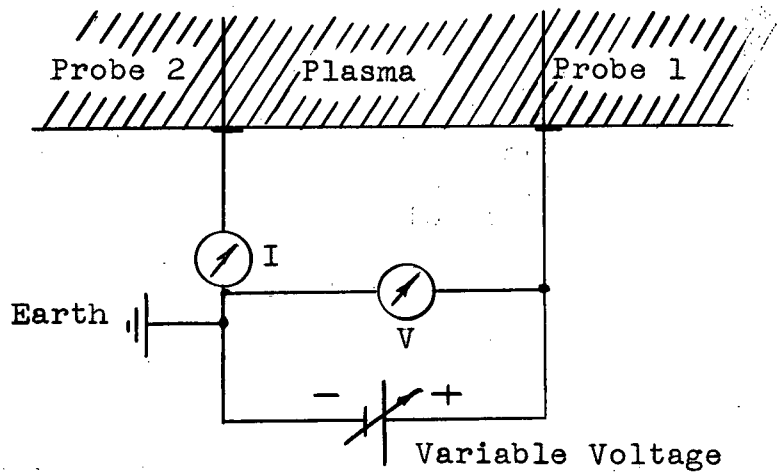

FIGURE 1.2 DOUBLE PROBE CIRCUIT WITH ONE GROUNDED PROBE

No current will flow between the probes since the random electron and ion currents to each are the same, assuming that there is no temperature gradient between the probes, which is likely to be true in a decaying plasma. If a voltage V is applied between the probes such that probe 1 becomes positive, the electrons are attracted to probe 1. This leaves a deficiency of electrons in the region between the probes, hence the plasma potential rises. In other words, the plasma assumes a potential approximately the same as the most positive electrode with which it makes contact. This means that the grounded probe (probe 2) is at a negative potential with respect to the plasma. By Kirchhoff's laws, the current registered by the ammeter will be controlled by the number of positive ions striking probe 2, or the number of electrons striking probe 1 and flowing in the external circuit to probe 2, whichever is smaller. As the voltage between probes 1 and 2 is increased, eventually voltage V_s is reached when enough electrons strike probe 1 to equalize the number of ions striking 2. This is not necessarily the positive ion drift current because probe 2 is connected to ground, i.e. the probe circuit is not floating. Because the plasma is in contact with the chamber walls and also the main spark gap electrodes, which during the afterglow are at ground potential, the potential distribution in the plasma is distorted from the case where the probe circuit floats. Further increase in the voltage between the probes, beyond V_s, should cause little

increase in the current flowing in the external circuit, and probe 2 is saturated, i.e. it collects all the positive ion current. This saturation point shows as the "knee" in the current waveform.

Around probe 2 there is even a greater deficiency of electrons now that $V \neq 0$ than there was when $V = 0$. This is due to the accelerating field (for electrons) which is now present between the probes. Hence, when V is greater than zero most of the voltage impressed between the probes appears as a voltage drop across the positive ion sheath. The existence of this positive ion sheath around probe 2 was verified experimentally by covering a portion of the exposed area of both probes 1 and 2 with an insulating sleeve. The results were as follows:

a. with no sleeve on either probe 1 or probe 2 the peak current I_{pl} flowed in the probe circuit

b. with the insulating sleeve covering a given fraction of the area of probe 1, the peak current was I_{pl}

c. with the insulating sleeve covering a given fraction of the area of probe 2, the peak current was I_{pl} reduced by this fraction

d. with the insulating sleeve covering a given fraction of the area of both probes 1 and 2, the peak current was I_{pl} reduced by the fraction of the area of probe 2 which was covered.

All these steps were carried out under the same experimental conditions, and the shape of the current waveform remained constant, independent of the exposed probe areas. Only the magnitude of the current waveform changed. One can therefore conclude that it is the area of probe 2 which controls the magnitude of the current in the probe circuit. In other words, by reducing the exposed area of probe 2, the size of the positive ion sheath and the number of positive ions collected are reduced proportionately.

Around probe 1 the positive ion sheath, which was present when the voltage between the probes was zero, is no longer present because of the influx of electrons to this probe. Figure 1.3 shows the potential diagrams for the probes.

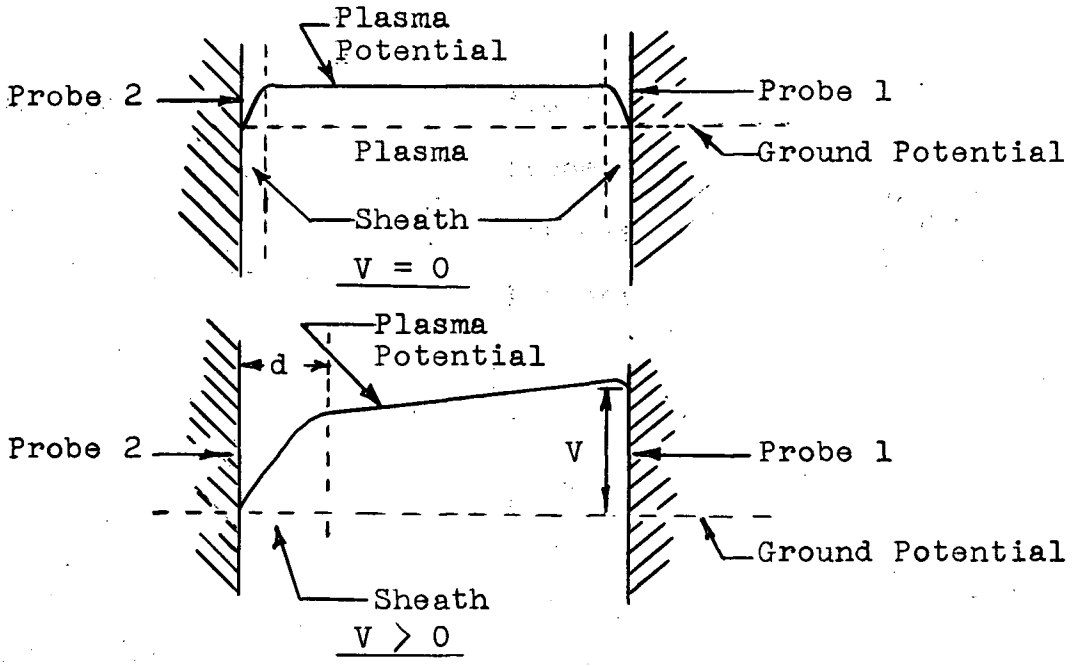

FIGURE 1.3 PROBE POTENTIAL DIAGRAMS WITH PROBE 2 GROUNDED

The preceding two diagrams look very much like the potential diagrams for the floating double probes described by Johnson and Malter (1950). The main features of the potential diagrams for both the floating double probes and the double probes, where one probe is grounded, are the same. For the exact mathematical analysis of Johnson and Malter (1950) to be applicable, however, the probes must be floating.

From the preceding analysis of plasma sheaths it is evident that the field between the probes is not given by $\frac{V}{a}$

where: V = voltage applied between the probes (volts)

a = distance between the probes (meters)

or even closely approximated by it. Assume that the whole voltage V applied between the probes appears across the sheath at probe 2, which is a good assumption if V is greater than $\frac{kT}{q_e}$, and approximate the voltage gradient by a linear function. The field E across the sheath is then (see Figure 1.3)

$$E = \frac{V}{d} \quad (\text{volts meter}^{-1})$$

where: V = voltage between the probes (volts)

d = sheath thickness (meters).

Assuming that the probes are cylindrical, the area of the sheath A_s (which is the area collecting ions) is:

$$A_s = 2\pi(r + d)\ell \quad (\text{meters}^2)$$

where: r = probe radius (meters)

ℓ = probe length (meters).

The current I flowing through the ammeter is:

$$I = J_i A_s \quad \text{(amps)}$$

where the positive ion current density at saturation is given by:

$$J_i = \frac{I_s}{2\pi(r + d)\ell} \quad \text{(amp meter}^{-2}\text{)}$$

and: I_s = ammeter current at saturation (amps).

The positive ion conductivity σ_i is given by:

$$\sigma_i = \frac{J_i}{E} \quad \text{(mho meter}^{-1}\text{)}$$

$$= \frac{I_s \, d}{2\pi(r + d)\ell V}$$

or: $$\sigma_i = G \frac{1}{2\pi\left(\frac{r}{d} + 1\right)\ell}$$

where the probe conductance G is given by:

$$G = \frac{I_s}{V_s} \quad \text{(mho)}$$

and: V_s = voltage between the probes at current saturation.

The conductivity, as it is usually defined, is calculated by taking into account electron motion only. The ratio of the conductivity due to electrons, to the conductivity due to ions is proportional to the ratio of the electron velocity to the ion velocity. Where the electrons and ions are at the same temperature, these velocities are inversely proportional to the square root of the particle mass. Hence, assuming that the ions are only singly charged, which is reasonable, as the temperature

is at most a few electron volts, then the conductivity σ is:

$$\sigma = \sigma_i \left[\frac{M}{m}\right]^{1/2} \quad \text{(mho meter}^{-1}\text{)}$$

$$= G \frac{1}{2\pi\left(\frac{r}{d} + 1\right)\ell}\left[\frac{M}{m}\right]^{1/2} \qquad \ldots 5$$

where: M = ion mass (kg)

m = electron mass (kg).

In his book, Spitzer (1956) gives the following formula for the conductivity σ of a highly ionized gas:

$$\sigma = 1.53 \times 10^{-2} \frac{T^{3/2}}{\ln \Lambda} \quad \text{(mho meter}^{-1}\text{)} \qquad \ldots 6$$

where: T = temperature (^{o}K)

Λ = ratio of the Debye shielding distance to the impact parameter for 90^{o} collisions.

If one assumes that this formula holds for a weakly ionized plasma, as is the case here, at least in the latter part of the recovery period, then the two values for σ in equations 5 and 6 can be equated. The values of $\ln \Lambda$ change very slowly with changes in temperature and electron density (see table 5.1, Sptizer). The sheath thickness d should also be relatively constant with changes in T as the voltage V_s, which is the probe voltage at current saturation, is always much greater than $\frac{kT}{q_e}$ in this experiment. Therefore, V_s rather than T will determine the sheath thickness. Because $\ln \Lambda$ and d can be considered constant, the preceding analysis shows that the

probe conductance G is proportional to the conductivity σ, which in turn is proportional to the three-halves power of the temperature. Hence:

$$G = KT^{3/2} \quad \text{(mho)} \qquad \ldots 7$$

where the constant K is:

$$K = \frac{9.6 \times 10^{-2} \left(\frac{r}{d} + 1\right) \ell}{\ln \Lambda} \left[\frac{m}{M}\right]^{1/2} \quad \left(\text{mho } {}^{o}K^{-3/2}\right)$$

Now, if it is possible to calculate K or to experimentally determine it, then the temperature can be deduced from the measured probe conductance. The accuracy of this calculated temperature, (which will be considered in detail in Chapter 5, Discussion of Results), will depend primarily on whether K is really constant throughout the range of experimental conditions investigated.

The analysis indicates that it is immaterial, in this experiment, whether the field in the sheath varies linearly or not, so long as the form of the field does not change in time or throughout the experiment. The field was assumed to vary linearly as this assumption led to a simple analysis of the field and the possibility that an estimate of the constant K might be obtained from experimental values of the sheath thickness d and the parameter Λ.

CHAPTER 2: DEVELOPMENT OF APPARATUS

2.1 GENERAL DESCRIPTION AND OPERATION OF APPARATUS

Figures 2.1 and 2.2 are block diagrams of the apparatus. With reference to these diagrams, the operation of the apparatus is as follows. The nominal 9 μF high voltage capacitor bank is charged to 20 kV from the variac controlled E.H.T. set. The discharge is initiated by a pulse from the control panel. The magnetic field associated with the rapidly rising current in the high current generator circuit, induces a voltage in a small pick-up coil (visible in Figure 2.5) which is proportional to the rate of change of current in the main discharge circuit. This voltage triggers a delay unit which, after some set delay, triggers the sawtooth generator which generates a single waveform. The sawtooth wave passes through a cathode follower (CF) and from thence to the probes. The current and voltage flowing in the probe circuit are displayed on a Tektronix type 551 double beam oscilloscope which is also triggered from the output of the delay unit.

The construction of the apparatus is shown in Figures 2.3 to 2.6. This system is similar in principle to that described by Churchill, Parker and Craggs (1961) and Chan (1963). The main spark chamber is a 6 inch inside diameter cross made

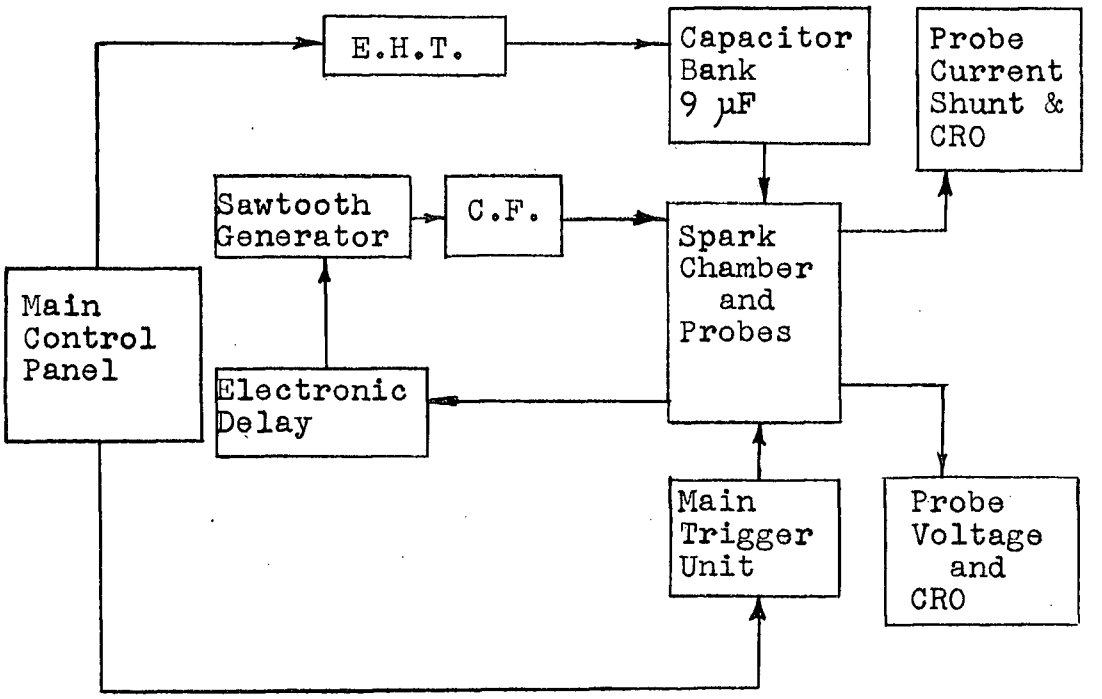

FIGURE 2.1 BLOCK DIAGRAM OF APPARATUS

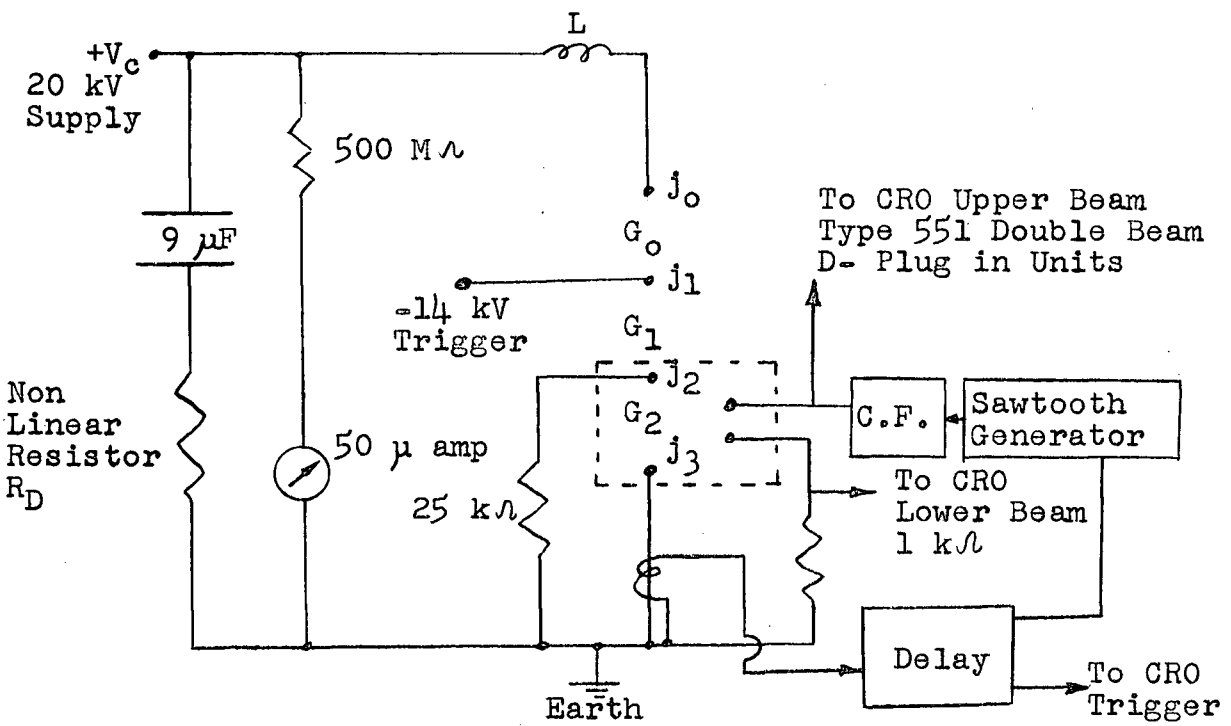

FIGURE 2.2 OVERALL CIRCUIT DIAGRAM

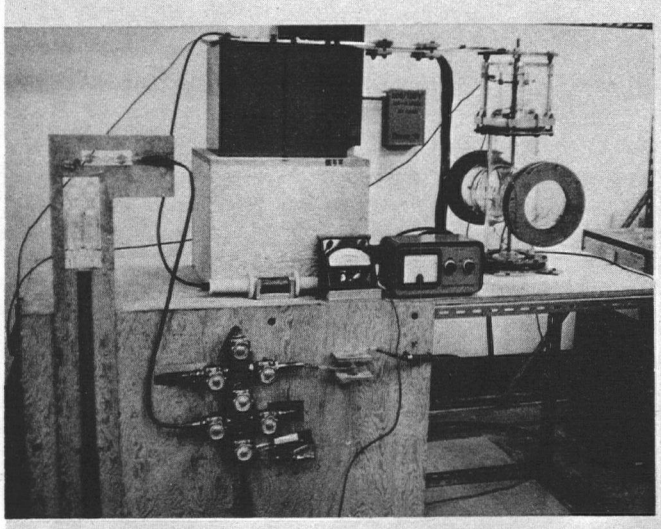

FIGURE 2.3 OVERALL VIEW OF APPARATUS

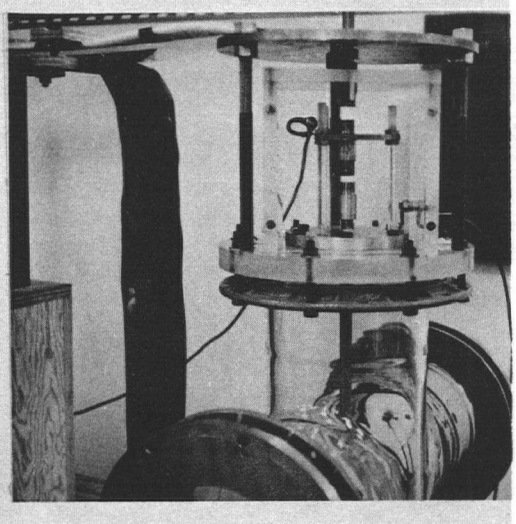

FIGURE 2.4 TRIGGERING ELECTRODES AND SPARK GAPS G_o AND G_1

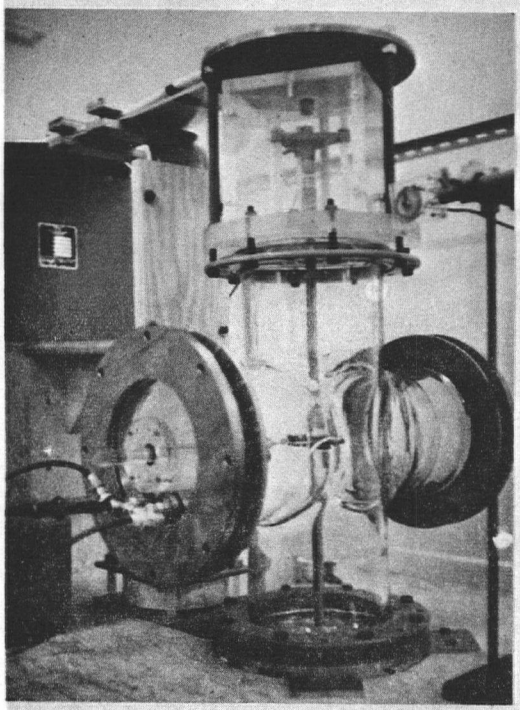

FIGURE 2.5 SPARK CHAMBER AND PROBES

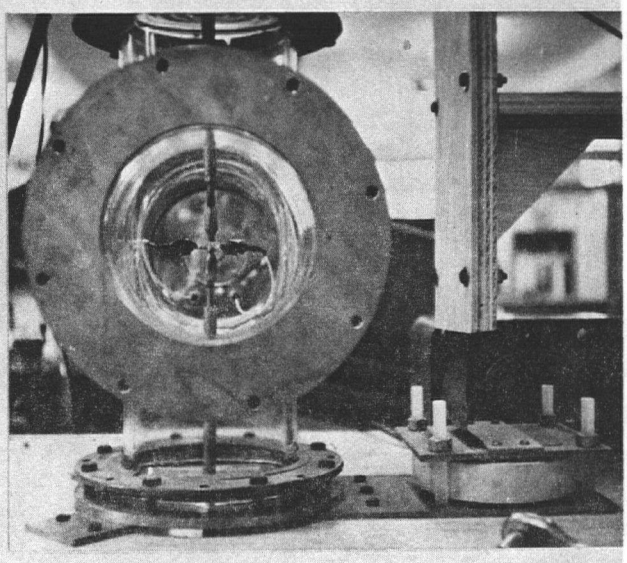

FIGURE 2.6 MAIN ELECTRODES j_2 AND j_3 AND PROBES

of pyrex glass and can be evacuated. The main electrodes are 6.4 mm diameter tungsten slugs, the ends machined flat, and mounted in brass holders. The distance between the electrodes can be varied by screwing the electrode tip into the supporting shaft (see Figure 2.6). The trigger electrodes (see Figure 2.4) are 16 mm diameter tungsten slugs and the whole trigger gap mechanism is mounted inside a tight fitting perspex box in order to reduce noise.

2.2 VACUUM SYSTEM

In order to facilitate experiments at pressures less than atmospheric, it is possible to evacuate the spark chamber. The vacuum is created by a Phillips Duo 5 two stage rotary vacuum pump with a pumping speed of 1.5 liters per second. Using conventional "O" ring vacuum seals at the joints, the system has a base pressure of about 10 μ Hg. There is a needle valve fitted to the system so that a controlled leak can be maintained.

Gas pressures are measured on the following instruments. For pressures down to about 10 mm Hg a mercury U-tube is used. Below this pressure two vacustats are employed, one from 0 to 10 mm Hg and the other from 0 to 1 mm Hg. Also, below 2 mm Hg the pressure can be continuously monitored by a Pirani, vacuum gauge type GP-110 which has two ranges, one from 0 to

2000 μHg and the other from 0 to 50 μHg and is calibrated from the vacustats.

2.3 HIGH CURRENT GENERATOR AND TRIGGERING MECHANISM

The high current generator is composed of two 4.5 μF, low inductance capacitors (NRG type 201) connected in parallel and charged through an E.H.T. power supply to V_c. These capacitors are discharged through the spark gaps. The discharge circuit is critically damped with a non-linear resistor (6 inch diameter morganite resistor type 801) in order to produce a unidirectional current pulse. The non-linear resistor is used as it produces a higher peak current than does a linear resistor. In the four electrode gap assembly the gap G_o is set so that it will not break down on application of V_c but will break down when the negative trigger pulse is applied. G_1 and also the main gap G_2 are set to break down upon application of V_c.

The high current generator is triggered by a negative pulse applied to electrode j_2. The pulse is generated in the following manner (see Figure 2.7). The anode of the trigatron is charged to +14 kV through the potential divider composed of the 50 MΩ and 120 MΩ resistors which are connected across the main bank. A 10 kV pulse from the pulse transformer causes the trigatron to break down and drop its anode potential to zero. This process applies a negative pulse of 14 kV to

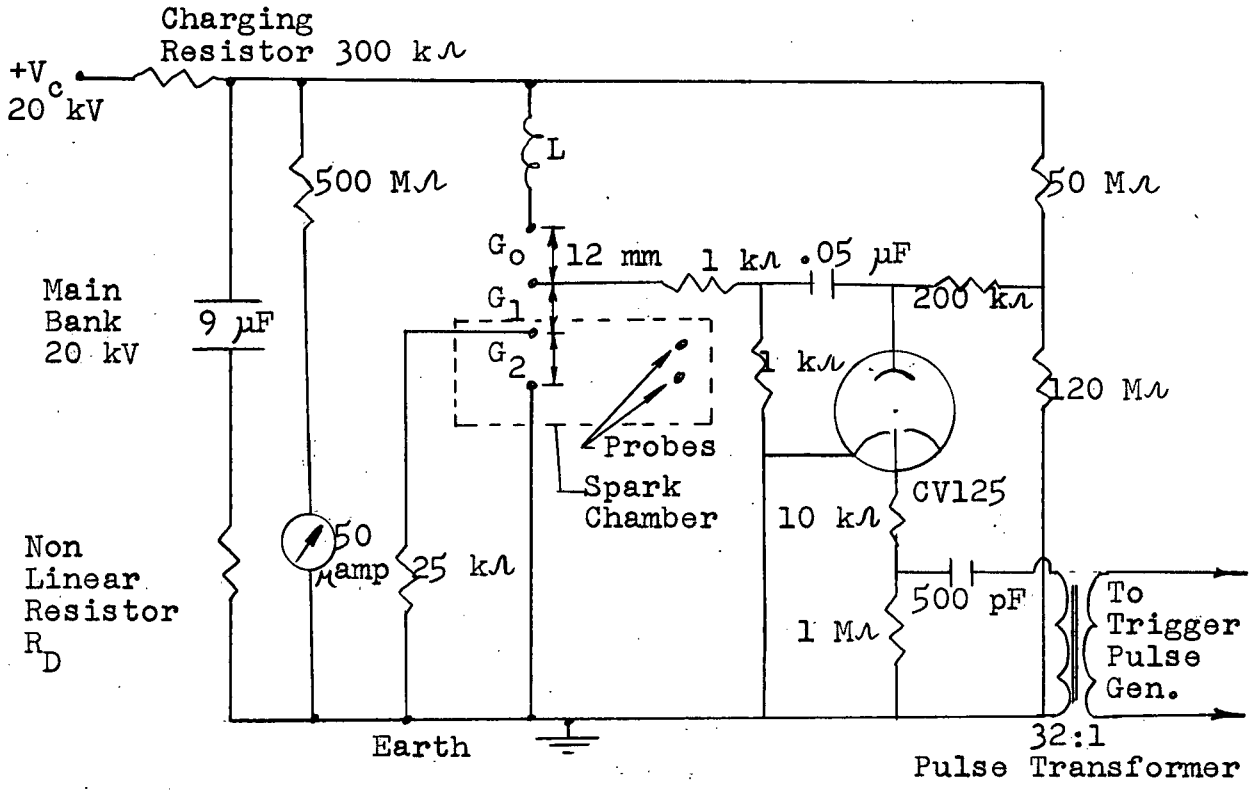

FIGURE 2.7 HIGH CURRENT GENERATOR AND TRIGGER CIRCUITS

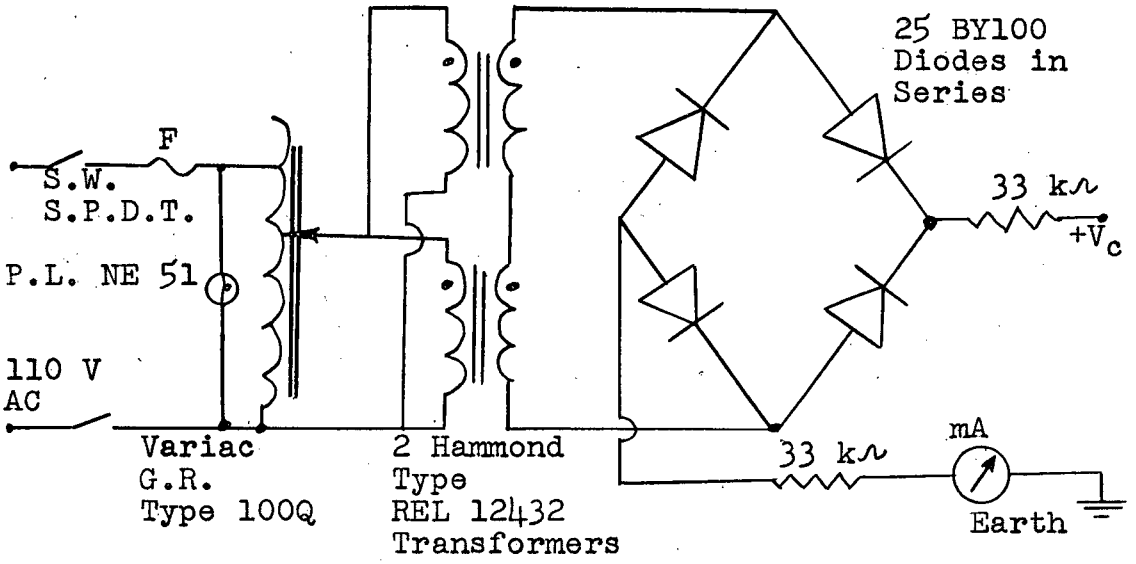

FIGURE 2.8 E.H.T. SUPPLY

electrode j_2 and gap G_o breaks down initiating the discharge.

The circuit diagram for the E.H.T. power supply is shown in Figure 2.8. This supply is simply a full wave rectifier, each arm of which is composed of twenty-five BY 100 diodes connected in series and shown schematically by a single diode. The maximum current which can be drawn from this supply is 200 mA.

Because there is often some delay in the trigger circuit, all the electronic apparatus is triggered from the output of a small pick-up coil. As stated previously, the voltage produced by this coil is proportional to $\frac{dI}{dt}$. Hence the output of this coil can be used to determine the parameters of the circuit. With the resistor R_D shorted out the period of the ringing discharge determines the overall circuit inductance L. For low values of stray circuit resistance

$$L = \frac{T^2}{4\pi^2 C} \quad \text{(henry)}$$

where: T = period of ringing discharge (sec.)

C = capacitance of system = 9 μF.

By electrically integrating the $\frac{dI}{dt}$ pulse, a pulse proportional to the discharge current is obtained. Because the area under the current vs. time curve is equal to the original charge stored in the capacitor bank, CV_c, the constant of

proportionality can be deduced. Current and $\frac{dI}{dt}$ waveforms are shown in Figures 2.9a, b, and c. Table II lists the parameters of the high current generator.

TABLE II CIRCUIT PARAMETERS

Parameter	Value
Number of capacitors	2
Capacitance of each capacitor	4.5 μF
Working voltage	20 kV
Maximum energy	1.8 kJ
Total circuit inductance	0.86 μH
Peak current	25 kA

2.4 TRIGGER PULSE GENERATOR (FIGURE 2.10)

The unit usually operates with a micro-switch connected to the manual input. This switch, when depressed, connects the grid of the 2D21 tube through 100 kΩ to ground. This fires the tube yielding a positive pulse at the cathode and a balanced output across 1 MΩ at the anode. The pulse from the anode goes to the pulse transformer in the main bank trigger circuit and thence initiates the discharge.

2.5 ELECTRONIC DELAY UNIT (FIGURE 2.11)

This is essentially a monostable multivibrator which

Time ⟶

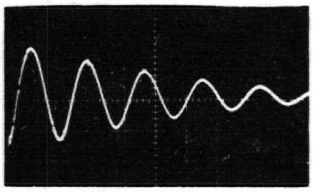

FIGURE 2.9a $\frac{dI}{dt}$ WAVEFORM FOR RINGING DISCHARGE
Time 10 μs/div

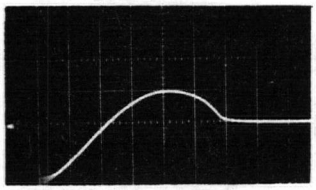

FIGURE 2.9b $\frac{dI}{dt}$ WAVEFORM
Time 2 us/div

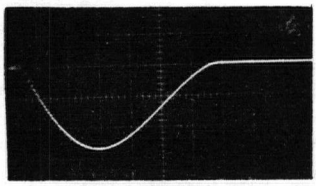

FIGURE 2.9c I WAVEFORM
Time 2 us/div
Peak current = 25 kA

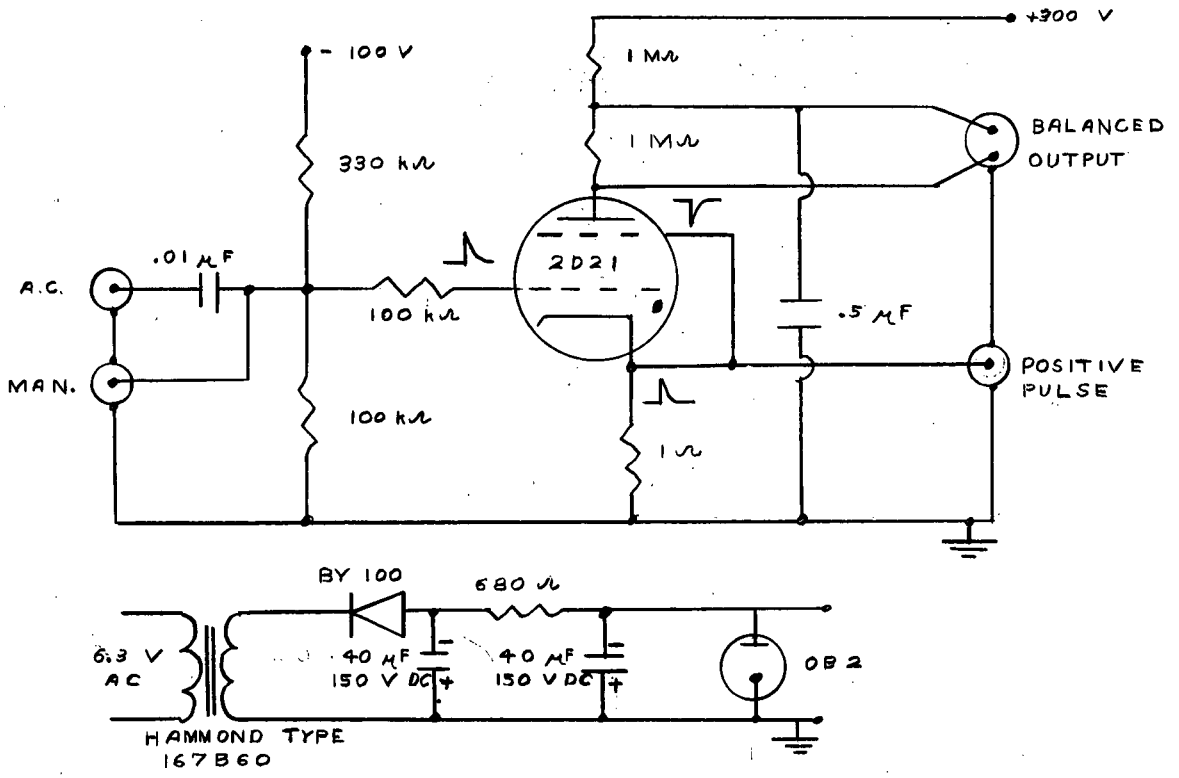

FIGURE 2.10 TRIGGER PULSE GENERATOR

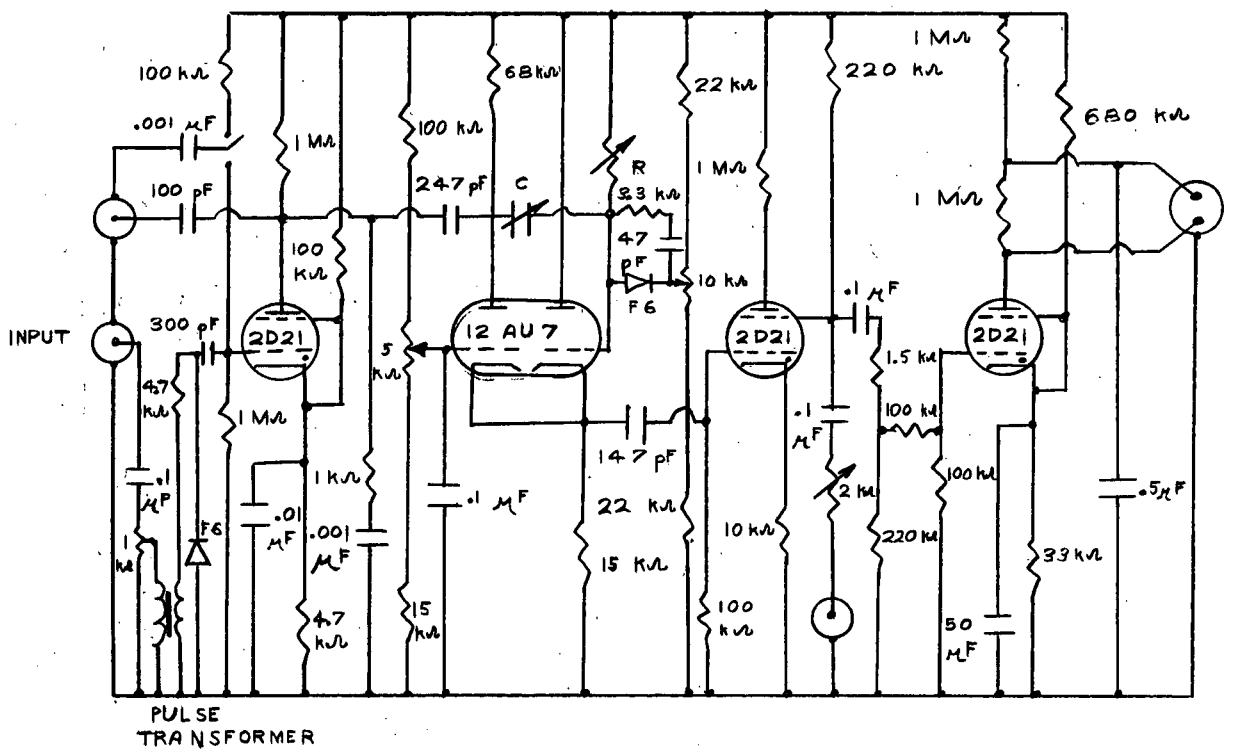

FIGURE 2.11 ELECTRONIC DELAY UNIT

generates delays controlled by the R-C time constant of the circuit. With this unit, delays are available for a range of 5 decades with ten steps per decade. The delay times range from 100 μs to 10 sec.

The main bank current rise generates a pulse in the pick-up coil. This pulse is then used to trigger the delay unit. The output of the delay unit triggers the recording oscilloscope and the sawtooth pulse generator.

The delay unit is calibrated by means of an oscilloscope to an accuracy of approximately 2%.

2.6 PROBE DEVELOPMENT AND ASSOCIATED CIRCUITRY

The probe circuitry is shown in block form in Figures 2.5 and 2.6 and is shown in the form which was finally adopted for this experiment in Figure 2.12. A Tektronix 515 oscilloscope serves as the sawtooth pulse generator. The 515 oscilloscope was chosen for the generator primarily because it was readily available, it could supply a sawtooth pulse with a rise time from 2 μs to a number of seconds and a peak amplitude of 150 volts, and it could be triggered easily.

The voltage between the probes and the current flowing in the probe circuit were displayed on the upper and lower beams respectively of a type 551 double beam oscilloscope with type D

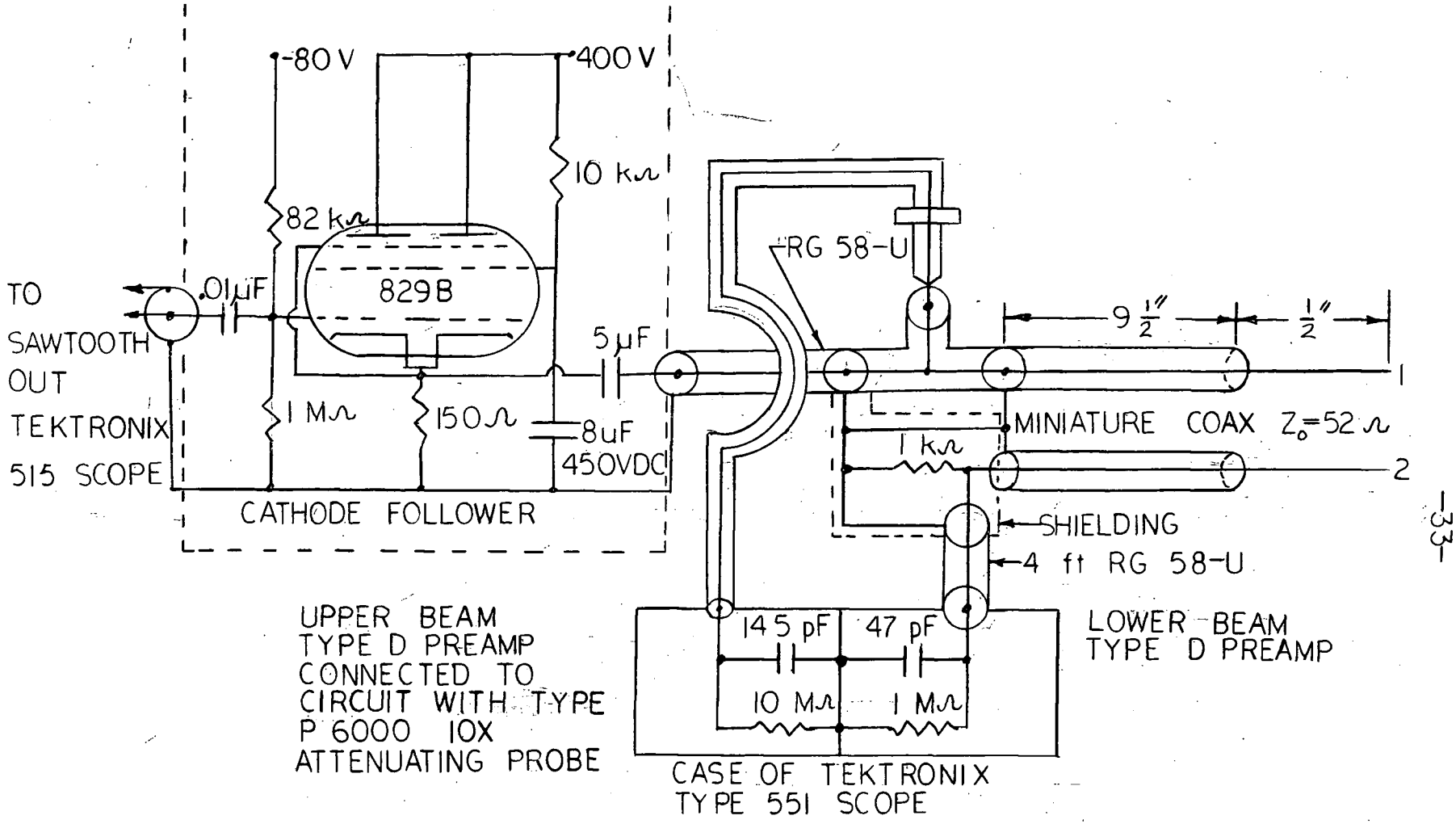

FIGURE 2.12 DETAILED PROBE CIRCUIT

preamplifiers and were recorded on polaroid film. The voltage between probe 1 and ground (see Figure 2.12) was measured with a ten times attenuating probe (Tektronix type P 6000, which has a frequency response of dc to 30 Mc). The small correction necessary to account for the potential drop across the 1 kΩ current shunt is negligible, hence, the upper beam displayed directly the voltage between the probes. The current was measured as a potential drop across a 1 kΩ, one percent carbon deposit resistor. The type D preamplifier was used because of its high sensitivity. The sensitivity of this preamplifier is 1 mV/div to 50 volts/div calibrated, and the frequency response is dc to 300 kc at 1 mV/div sensitivity, increasing to dc to 2 Mc at 50 mV/div and lower sensitivities. This narrow pass band might appear to severely limit its usefulness. Experimentally, however, it was found that the preamplifier did not introduce any noticeable distortion in a sawtooth pulse of 10 μs risetime. Throughout most of the experiment a pulse with a risetime of 10 μs was used and hence this preamplifier was acceptable.

The manner in which the probes were shielded and the details of the probe circuit evolved as solutions to numerous problems were obtained. Measurements of very small currents, which are flowing at the same time as very large currents, or even a short time after the large current pulse has ceased, are

difficult to make. In this experiment the main current pulse was about 10^4 amps while the currents in the probe circuit were from 10^{-6} to 10^{-4} amps, a difference of 8 to 10 orders of magnitude. When the main bank discharged, the changing magnetic field associated with the current pulse induced large (500 to 1,000 volts) voltages in the probes and as a result large currents flowed in each probe. The oscilloscope preamplifiers, which were set at high gain, became saturated. It then required a finite time for these preamplifiers to desaturate so that waveforms were again accurately displayed on the oscilloscope. The length of time required for these preamplifiers to desaturate depended upon the magnitude of the pulse induced by the main discharge and the gain settings of the preamplifiers. In practice this means that measurements can not be made for times less than 0.2 ms after the discharge. If one were interested in investigating this region of time delays, some kind of gating circuit would have to be used whereby the probes could be disconnected from the measuring circuit while the main discharge was taking place.

This pick-up pulse would also cause the sawtooth generator (515 oscilloscope) to trigger prematurely. In the experiment this problem was cured relatively easily by inserting a cathode follower stage between the trigger generator and the probes. This cathode follower isolated the generator from the probes.

The voltage across the probes was pulsed and hence the current flowing in the probe circuit was also pulsed. Because of the pulsed nature of the voltage, stray capacitances in the circuit had to be carefully balanced or eliminated. The capacitance between each probe and ground had to be the same and direct capacitance between the probes was, as far as was possible, eliminated. If this was not done, the voltage across the 1 kΩ current shunt, when the probes had infinite impedance between them, was the differential of the voltage applied between the probes.

Closely related to the problem of signal differentiation was the problem of noise pick up. By maintaining coaxial symmetry, as far as possible, and by shielding all parts of the circuit, a clean current waveform could be obtained. The probes were shielded coaxially to within $\frac{1}{2}$ inch of their tips. In order to maintain coaxial symmetry in the probe circuit a coaxial vacuum connector was used to pass through the walls of the spark chamber (see Figure 2.5). The cathode follower also served to reduce the overall noise of the circuit by changing the high output impedance of the sawtooth generator to a low impedance of about 100 ohms.

After all these precautions were taken, the oscilloscope indicated zero current flowing in the probe circuit upon application of the voltage sawtooth when there was infinite

impedance between the probe tips. When a resistor of 2 MΩ was connected between the probe tips, the current waveform exactly followed the voltage and the current was the expected 75 μamp for an applied voltage of 150 volts. The 1 kΩ current shunt was experimentally chosen from values between 100 ohms and 100 kΩ to produce the cleanest current waveform when various resistances were connected between the probe tips.

The final design of the probes used in this experiment is shown in Figure 2.13. The original set of probes were made of two pieces of platinum wire, 0.5 mm in diameter, 1 cm long and oriented parallel to each other with a separation of 5 mm. These probes were used for the preliminary investigations, but had two disadvantages, namely, the platinum wire lacked rigidity and, as the probe wires were parallel, the capacitance between the two probes was high. In the final design tungsten wire was chosen for the probe material because of its strength, high melting point, and its resistance to erosion and sputtering. At the conclusion of the experiment the probes were viewed under a microscope and appeared to have suffered little damage from sputtering or erosion. The main spark gap electrodes were also tungsten and in this way the tungsten probes eliminated the problem of probe contamination from metal vapour boiled off the main electrodes during the discharge. The small wire size (0.5 mm in diameter) minimized the cooling effect of the probes on the plasma. The probes were oriented

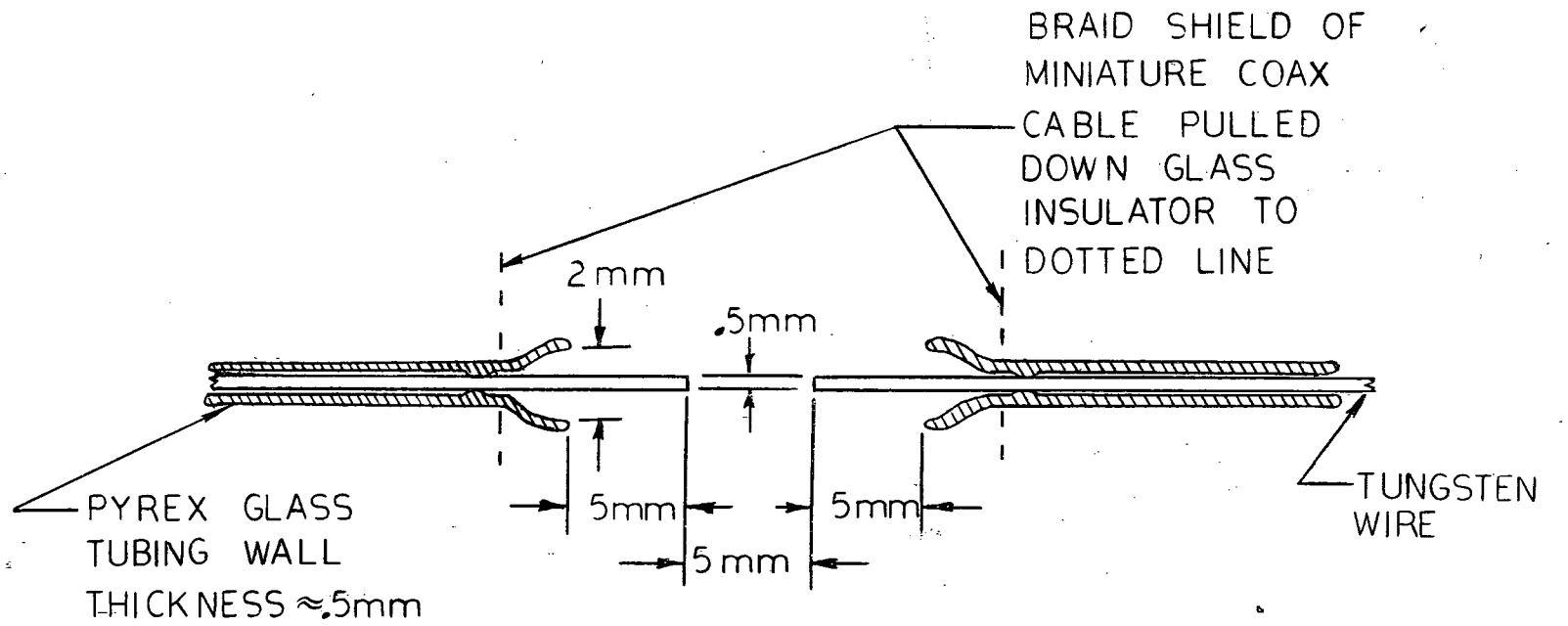

NOT TO SCALE

FIGURE 2.13 PROBE DIMENSIONS

in a horizontal plane and were co-linear with a distance of 5 mm between the tips. This orientation reduced the probe to probe capacitance considerably over that of the original platinum probes. The probes were mounted on brackets at the end of a lucite rod so that their radial position could be varied with respect to the test gap.

CHAPTER 3: MEASUREMENTS AND DATA

In this section the measurement methods are discussed, typical oscilloscope traces of current voltage vs. time are reproduced and discussed, and some comments are made on the recovery measurements which were used to supplement the probe conductance measurements.

3.1 CONDUCTANCE MEASUREMENTS

As was stated in Chapter 2, the conductance of the probes was deduced by applying a sawtooth shaped voltage pulse across the probes and measuring simultaneously the voltage and the current in the probe circuit. Even though measurements of this type do not disturb the recovering gas very much, there is still some disturbance, and so only one sawtooth pulse was applied at a set delay time after the main discharge took place. The complete conductance curve was obtained in a statistical manner. Each point is an average of three tests. Ideally many more tests (say 20) should be used to form an average, but the purpose of this experiment was primarily to deduce the usefulness of the probes and to determine experimental operating conditions.

The risetime of the sawtooth used in these conductance measurements is 10 μs. The rise time was chosen as it is short

compared to appreciable changes in the temperature, but long compared to the length of time for an ion to travel through the sheath surrounding probe 2. In order to determine that this risetime was not a factor in determining the conductance, runs were taken with sawtooth risetimes of 2 and 100 μs. The conductance determined from these runs was compared to that determined for 10 μs risetime, and, within experimental error, there was no difference, hence 10 μs was used. The sawtooth pulse attained a peak voltage of about 80 volts.

The radial distance between the probes and the main test gap was varied from 2 to 15 cm for gas pressures above 1 mmHg, and from 5 to 15 cm for gas pressures of 0.1 mmHg. The minimum distance was chosen so as to reduce the possibility of an arc forming between the main electrodes and the probes and subsequently damaging the probe circuit and the associated electronic circuitry.

The parameters which affect the main discharge were carefully controlled. Prior to, and following each run, the current and $\frac{dI}{dt}$ waveforms of the main discharge were taken and compared to previous records. The distance between the main electrodes was also checked during each run, as was the distance between the probes. A repetition rate of about one test per minute was chosen so that the non-linear resistor would not overheat and so that the air in the spark chamber would have

time to cool between tests. After every 15 to 20 tests the air in the chamber was changed.

For all gas pressures except 1 mmHg and 0.1 mmHg the gas pressure was static, but for these two the pressure was maintained by balancing the pumping speed against the controlled leak rate.

3.2 DATA OBTAINED

Measurements were made at different gas pressures and different radial distances from the axis of the test gap. The pressures chosen were 760, 200, 50, 10, 1, and 0.1 mmHg; the radial distances were 15, 10, 5, and 2 cm, except in the case of pressures of 0.1 mmHg where no measurements were made for a radial distance of 2 cm. Table III gives a summary of the data taken. There are certain values of pressure and radial distances which are not listed in this table. For these values there was no detectable current flow in the probe circuit for the range of delay time which could be investigated.

TABLE III RANGE OF EXPERIMENTAL CONDITIONS FOR WHICH PROBE CONDUCTANCE COULD BE MEASURED

Gas Pressure (mmHg)	Radial Dist. of Probes (cm)	Range of Delay Times (ms)	No. of Delay Times Used
200	2	0.25 - 2.2	5
50	2	0.39 - 3.0	7
10	2	0.25 - 6.6	7
	5	0.25 - 2.2	7
1	2	0.25 - 5.0	7
	5	0.25 - 16	10
	10	0.25 - 11	9
	15	0.34 - 16	10
0.1	5	0.34 - 5	7
	10	0.34 - 11	8
	15	0.34 - 11	8

One photograph, of the three taken for a complete run of data at a gas pressure of 1 mmHg and with the probes at a radial distance of 10 cm from the main gap, is shown in Figure 3.1. The voltage applied between the probes is recorded on the upper trace and the current on the lower trace. This series of photographs show a number of effects common to many or all the records. The expected current saturation is shown in all the photographs although for very small and very long delays the saturation effect is not as pronounced. It is also noticed that the current waveform is not the same shape during the time when the voltage is decreasing as it is while the voltage is increasing. This is presumably due to the fact that

For all photographs:
Voltage upper beam, current lower
Voltage scale = 50 volts/div.
Time base = 2 μs/div. increasing from right to left
Gas pressure = 1 mm.Hg
Probes 10 cm. from main gap

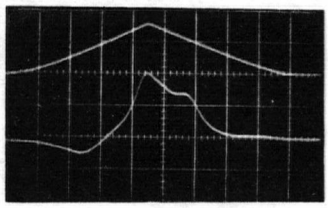

Delay =11 ms
Current=2 μamp/div

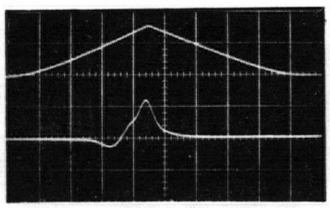

Delay =8.6 ms
Current=5 μamp/div

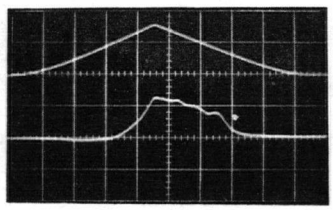

Delay =5.0 ms
Current=10 μamp/div

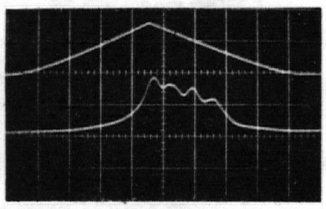

Delay =2.9 ms
Current=20 μamp/div

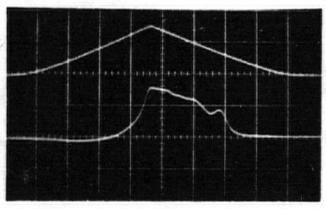

Delay =1.6 ms
Current=10 μamp/div

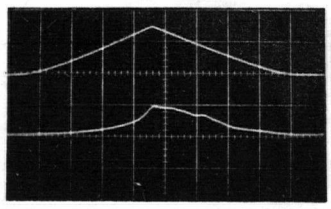

Delay =0.93 ms
Current=50 μamp/div

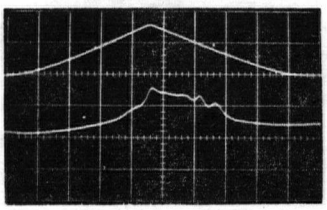

Delay =0.56 ms
Current=50 μamp/div

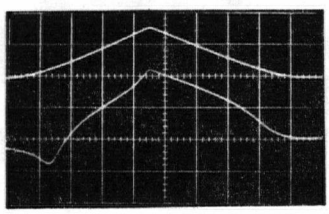

Delay =0.34 ms
Current=100 μamp/div

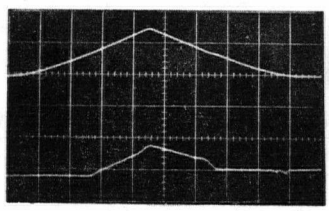

Delay =0.25 ms
Current=200 μamp/div

FIGURE 3.1 CURRENT AND VOLTAGE IN PROBE CIRCUIT

For all photographs:
Voltage upper beam, current lower
Voltage scale = 50 volts/div.
Time base = 2 μs/div. increasing from right to left

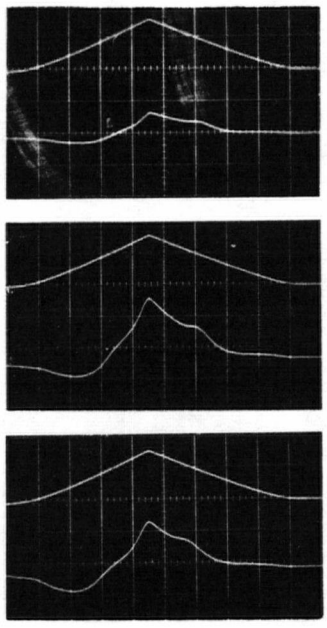

a.

b.

c.

Gas pressure = 1 mm.Hg
Probes 15 cm. from main gap
Delay = 5.0 ms
Current a. = 5 μamp/div.
b.,c. = 2 μamp/div.

FIGURE 3.2 CURRENT AND VOLTAGE VARIATION BETWEEN TESTS

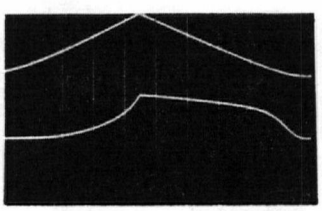

Gas pressure = 200 mm.Hg
Probes 2 cm from gap
Delay = 0.74 ms
Current = 50 μamp/div

FIGURE 3.3 CURRENT AND VOLTAGE FOR HIGH GAS PRESSURES

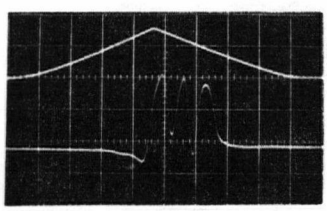

Gas pressure = 0.1 mm.Hg
Probes 10 cm from gap
Delay = 5.0 ms
Current = 10 μamp/div

FIGURE 3.4 LARGE OSCILLATIONS ON THE CURRENT WAVEFORM

the sheath surrounding the grounded probe acts as a small capacitor and stores electrical energy. This effect was not investigated in this experiment but under similar experimental conditions, Smy (1963) used this effect to estimate the sheath thickness. Superimposed on some of the current waveforms are oscillations. These oscillations only appear on the records taken at 1 and 0.1 mmHg gas pressure and for relatively long delay times. The amplitude of these oscillations is much larger at the lower pressure (see Figure 3.4). These oscillations, which are a relatively common phenomena in probe studies, occur because the plasma is disturbed by the probes. Loeb (1955) discusses this type of oscillation and shows that it occurs at the positive ion frequency ω_i,

$$\omega_i \approx \sqrt{\frac{n_i q_i^2}{M \epsilon_o}}$$

where: q_i = positive ion charge (coulombs)

n_i = positive ion density (ions meter^{-3})

M = ion mass (kg)

ϵ_o = permittivity of vacuum (farad meter^{-1})

For this experiment where oscillations occur an average value of the current is taken in computing the probe conductance.

In Section 3.1 it was pointed out that the current flowing in the probe circuit varies from discharge to discharge, even though the main discharge and the probe parameters remain

constant. Figure 3.2 shows three photographs with the same external parameters, in which the current is quite different from test to test. One explanation of this wide variation is that the main discharge itself is sometimes symmetric and sometimes not with the direction of the asymmetry completely random. Hence, at a given point in space, the measured conductance will be different from discharge to discharge. The asymmetry of the discharge channel is well established and has been recorded by Allen and Craggs (1954) with a rotating mirror camera.

3.3 RECOVERY MEASUREMENTS

Due to the extensive recovery work which has been done on similar apparatus, (Churchill, Parker, & Craggs, 1961; Churchill & Poole, 1963; Churchill 1961, 1963; Craggs, 1963; Chan, 1963) and as this technique is well developed, it was considered advantageous to determine the recovery characteristics of the main spark gap. This facilitates comparison between this apparatus and that used by the workers referred to above.

The recovery characteristics were derived by the method used by Churchill (1961) in which a unit function voltage is applied to the main gap electrodes at a given delay time after the main discharge has taken place. A fast oscilloscope,

connected to a potential divider which is across the main gap, enables one to determine if the gap reignites. The voltage of the unit function is varied until the minimum value which causes reignition is found. This is called the reignition voltage. The experimental apparatus and the detailed experimental method are the same as that used by Chan (1963) and are discussed in great detail in his thesis.

CHAPTER 4: ANALYSIS OF DATA

In this section the temperature will be derived from the probe conductance curves. The probe conductance for a gas pressure of 200 mmHg and delay time of 2 ms was measured experimentally. The gas temperature can be found from the reignition curves for these conditions, hence, the constant K (see equation 7) which relates the conductance G to the three halves power of the temperature can be found. When K is found or determined, the values of the probe conductance can be converted into temperatures.

4.1 DERIVATION OF TEMPERATURES FROM RECOVERY CURVES

During the latter part of the recovery the reignition voltage (V_R) obeys Paschen's law (Churchill, 1961; Chan, 1963) i.e. the reignition voltage is lowered due to decreased gas density. The manner in which the reignition voltage varies with gas density may be determined by measuring the impulse breakdown voltage as a function of gas pressure for the test gas at ambient temperature. Assuming that the test gas is a perfect gas and that it obeys a perfect gas law during reignition, and assuming that for a given reignition voltage the corresponding gas density is equal to the static gas density, then:

$$T_R = \frac{T\ P_R}{P} \qquad \ldots 8$$

where: T_R = recovering gas temperature (^oK)

T = ambient gas temperature (assumed = 300^oK)

P_R = ambient gas pressure (mmHg)

P = pressure, corresponding to the value V_R, which is found from the plot of the impulse breakdown voltage vs. ambient gas pressure (mmHg).

Figure 4.1 shows the plot of the impulse breakdown voltage vs. ambient gas pressure for 6.4 mm diameter tungsten electrodes, 0.5 cm apart, from which P is found. Figure 4.2 shows reignition curves for the 6.4 mm diameter main electrodes and Figure 4.3 shows the gas temperatures derived from equation 8. These curves agree, in general form, with those derived by Churchill (1961) and Chan (1963) under different experimental conditions.

4.2 RADIAL TEMPERATURES DERIVED FROM PROBE CONDUCTANCES

Measurements made by Chan (1963) show that the spark channel has a uniform temperature up to a radial distance of 2.5 cm at atmospheric pressure. Although the apparatus used by Chan (1963) was not identical to that used in this experiment they were very similar and it is reasonable to assume, in this experiment, that at a pressure of 200 mmHg the channel is

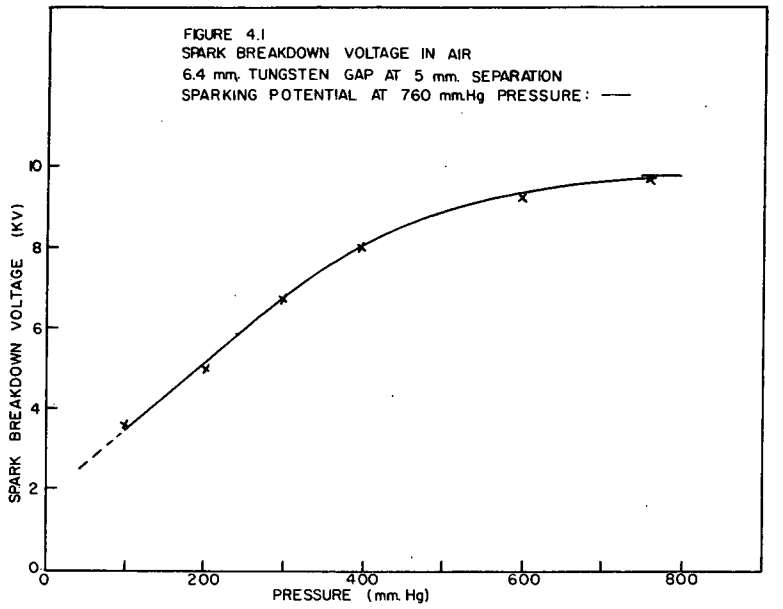

FIGURE 4.1
SPARK BREAKDOWN VOLTAGE IN AIR
6.4 mm. TUNGSTEN GAP AT 5 mm. SEPARATION
SPARKING POTENTIAL AT 760 mm.Hg PRESSURE: ——

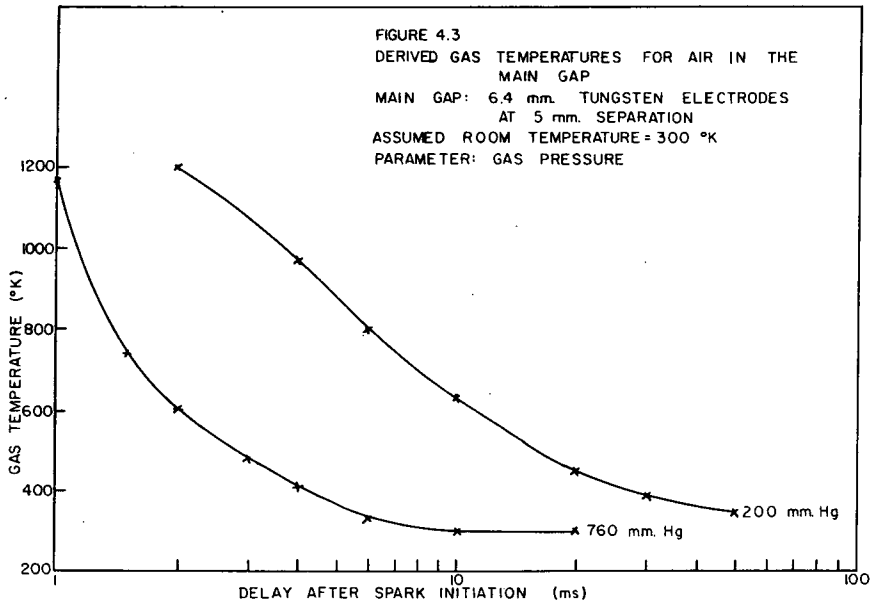

FIGURE 4.3
DERIVED GAS TEMPERATURES FOR AIR IN THE MAIN GAP
MAIN GAP: 6.4 mm. TUNGSTEN ELECTRODES AT 5 mm. SEPARATION
ASSUMED ROOM TEMPERATURE = 300 °K
PARAMETER: GAS PRESSURE

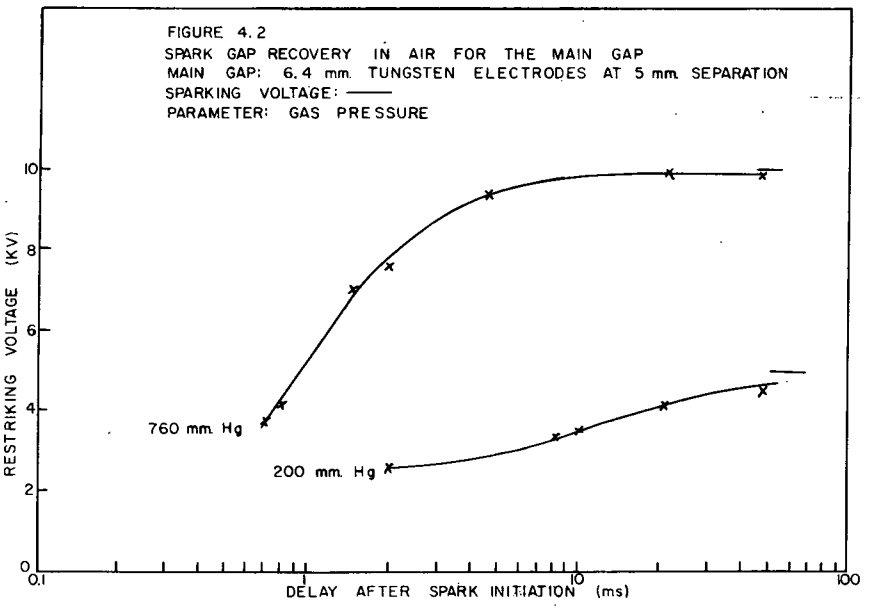

FIGURE 4.2
SPARK GAP RECOVERY IN AIR FOR THE MAIN GAP
MAIN GAP: 6.4 mm. TUNGSTEN ELECTRODES AT 5 mm. SEPARATION
SPARKING VOLTAGE: ——
PARAMETER: GAS PRESSURE

uniform out to a radial distance of at least 2 cm. This is especially true as the results in this experiment show that the spark channel radius increases with decreasing pressure. With this assumption, then, the temperature deduced from reignition measurements is the same as the temperature where the probes are located. Hence, for a pressure of 200 mmHg the observed conductance at a delay time of 2 ms and the measured temperature from reignition measurements are both known. The constant K of equation 7 is, therefore, calculated as:

$$K = 4.34 \times 10^{-13} \text{ mho } (^{o}K)^{-3/2}$$

or equation 7 is now:

$$G = 4.34 \times 10^{-13} T^{3/2} \qquad \ldots 9$$

Figures 4.4 to 4.7 show the probe conductance, which is the ratio of the current at saturation to the corresponding voltage, plotted against the delay time after spark initiation. Figures 4.8 to 4.11 show the temperatures which are derived from equation 9 and from the probe conductance curves. These results will be discussed in detail in Chapter 5.

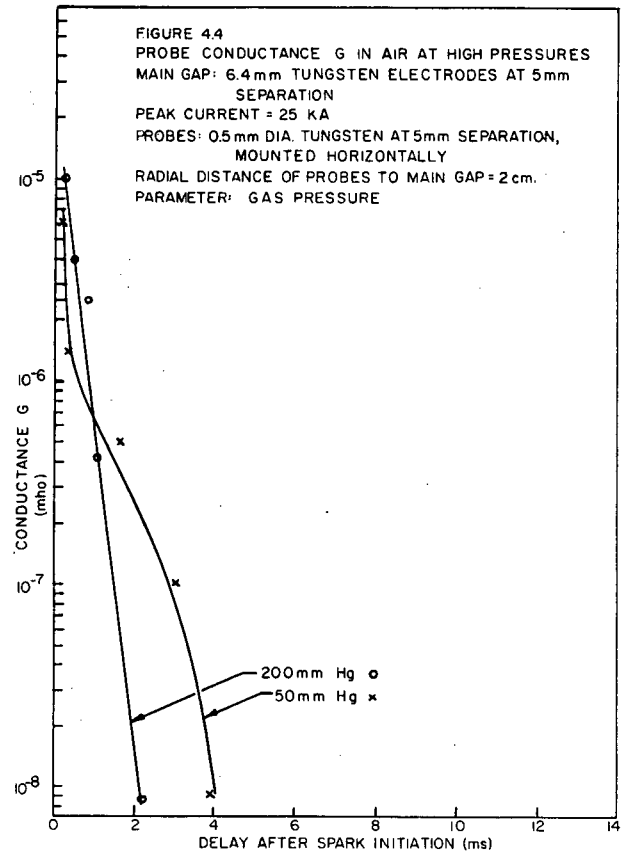

FIGURE 4.4
PROBE CONDUCTANCE G IN AIR AT HIGH PRESSURES
MAIN GAP: 6.4mm TUNGSTEN ELECTRODES AT 5mm SEPARATION
PEAK CURRENT = 25 KA
PROBES: 0.5mm DIA. TUNGSTEN AT 5mm SEPARATION, MOUNTED HORIZONTALLY
RADIAL DISTANCE OF PROBES TO MAIN GAP = 2 cm.
PARAMETER: GAS PRESSURE

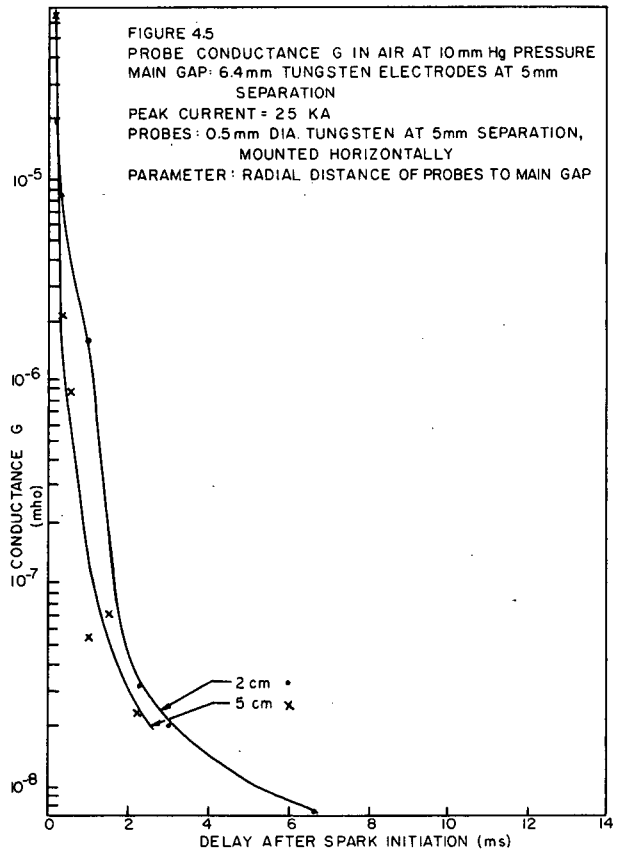

FIGURE 4.5
PROBE CONDUCTANCE G IN AIR AT 10mm Hg PRESSURE
MAIN GAP: 6.4mm TUNGSTEN ELECTRODES AT 5mm SEPARATION
PEAK CURRENT = 25 KA
PROBES: 0.5mm DIA. TUNGSTEN AT 5mm SEPARATION, MOUNTED HORIZONTALLY
PARAMETER: RADIAL DISTANCE OF PROBES TO MAIN GAP

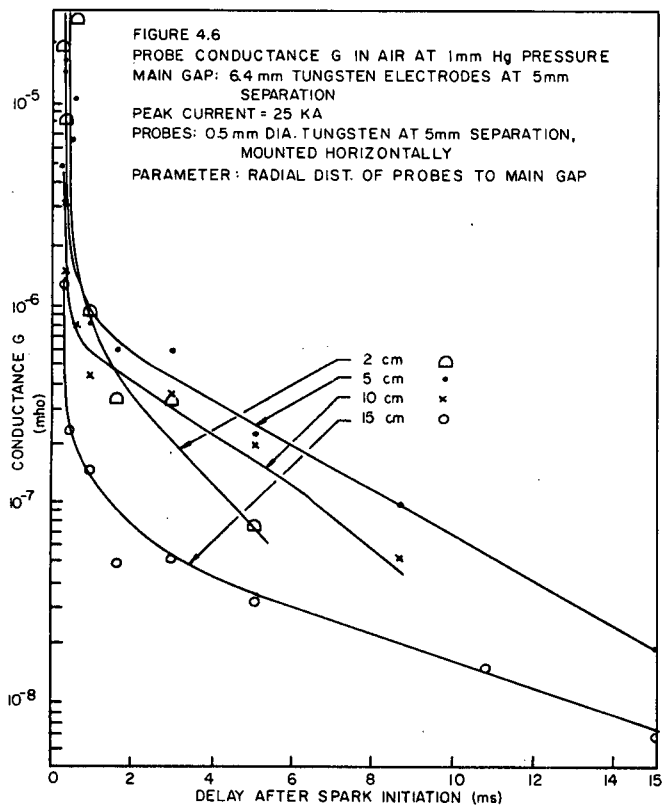

FIGURE 4.6
PROBE CONDUCTANCE G IN AIR AT 1mm Hg PRESSURE
MAIN GAP: 6.4 mm TUNGSTEN ELECTRODES AT 5mm SEPARATION
PEAK CURRENT = 25 KA
PROBES: 0.5 mm DIA. TUNGSTEN AT 5mm SEPARATION, MOUNTED HORIZONTALLY
PARAMETER: RADIAL DIST. OF PROBES TO MAIN GAP

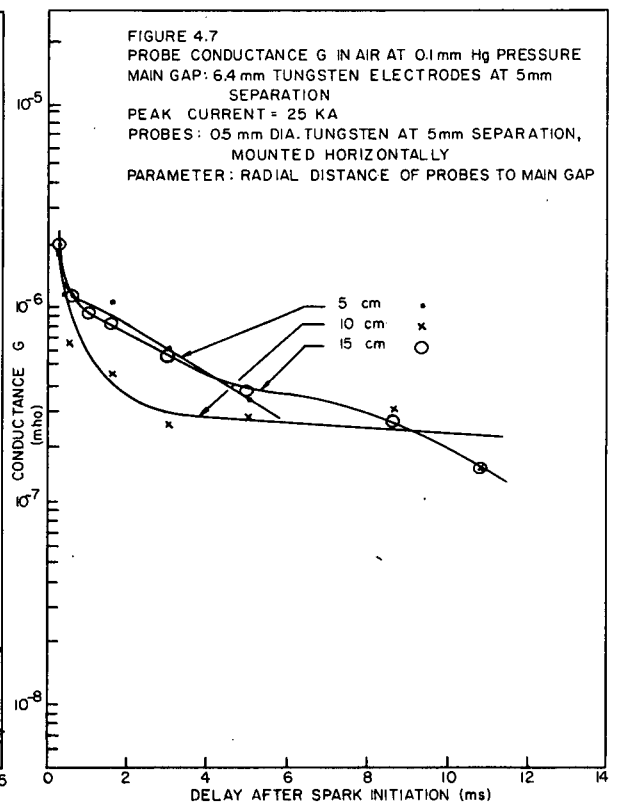

FIGURE 4.7
PROBE CONDUCTANCE G IN AIR AT 0.1mm Hg PRESSURE
MAIN GAP: 6.4 mm TUNGSTEN ELECTRODES AT 5mm SEPARATION
PEAK CURRENT = 25 KA
PROBES: 0.5 mm DIA. TUNGSTEN AT 5mm SEPARATION, MOUNTED HORIZONTALLY
PARAMETER: RADIAL DISTANCE OF PROBES TO MAIN GAP

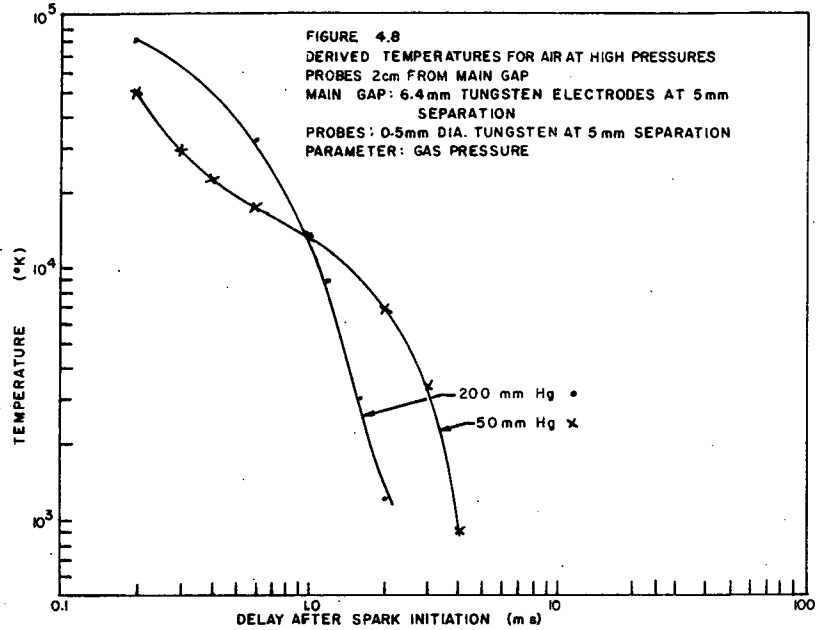
FIGURE 4.8
DERIVED TEMPERATURES FOR AIR AT HIGH PRESSURES
PROBES 2cm FROM MAIN GAP
MAIN GAP: 6.4mm TUNGSTEN ELECTRODES AT 5mm SEPARATION
PROBES: 0.5mm DIA. TUNGSTEN AT 5mm SEPARATION
PARAMETER: GAS PRESSURE
200 mm Hg •
50 mm Hg ×
TEMPERATURE (°K)
DELAY AFTER SPARK INITIATION (m s)

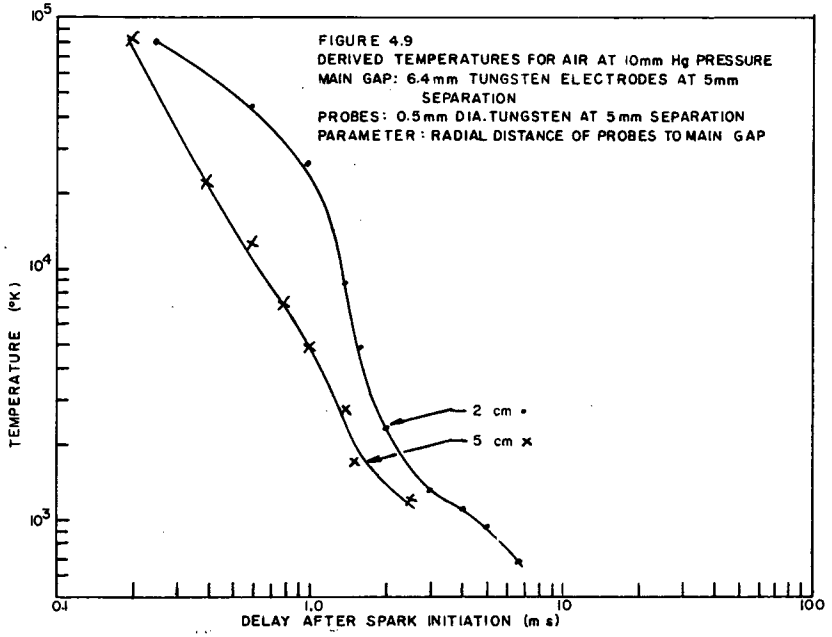
FIGURE 4.9
DERIVED TEMPERATURES FOR AIR AT 10mm Hg PRESSURE
MAIN GAP: 6.4mm TUNGSTEN ELECTRODES AT 5mm SEPARATION
PROBES: 0.5mm DIA. TUNGSTEN AT 5mm SEPARATION
PARAMETER: RADIAL DISTANCE OF PROBES TO MAIN GAP
2 cm •
5 cm ×
TEMPERATURE (°K)
DELAY AFTER SPARK INITIATION (m s)

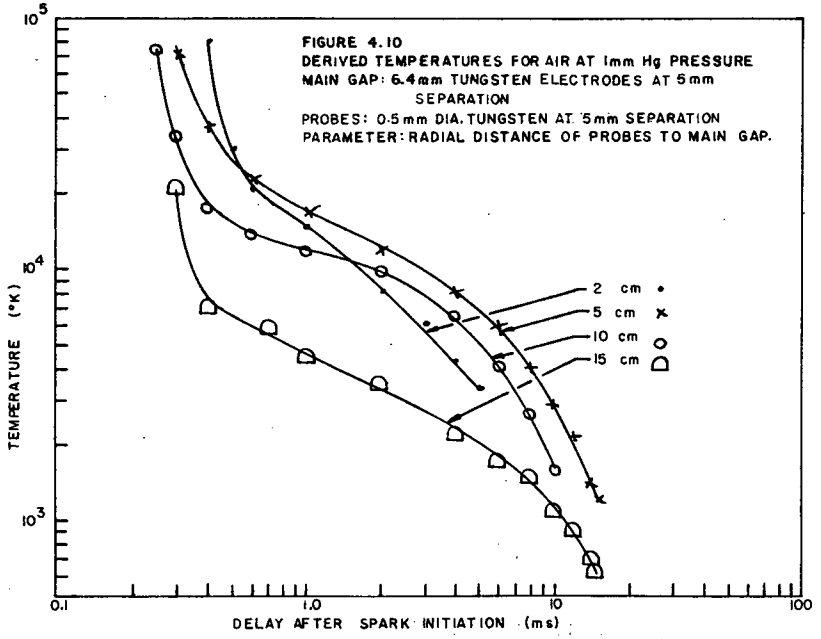
FIGURE 4.10
DERIVED TEMPERATURES FOR AIR AT 1mm Hg PRESSURE
MAIN GAP: 6.4mm TUNGSTEN ELECTRODES AT 5mm SEPARATION
PROBES: 0.5mm DIA. TUNGSTEN AT 5mm SEPARATION
PARAMETER: RADIAL DISTANCE OF PROBES TO MAIN GAP.
2 cm •
5 cm ×
10 cm ○
15 cm □
TEMPERATURE (°K)
DELAY AFTER SPARK INITIATION (ms)

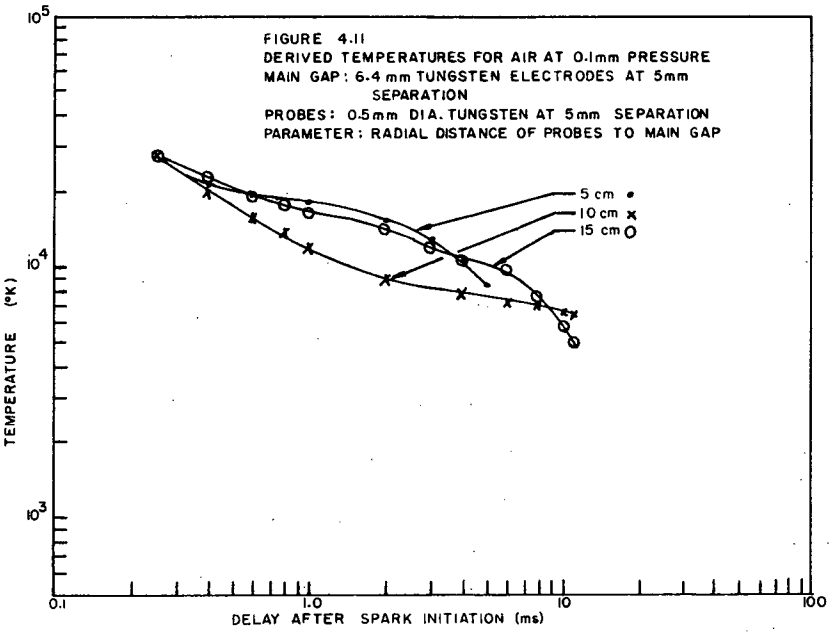
FIGURE 4.11
DERIVED TEMPERATURES FOR AIR AT 0.1mm PRESSURE
MAIN GAP: 6.4mm TUNGSTEN ELECTRODES AT 5mm SEPARATION
PROBES: 0.5mm DIA. TUNGSTEN AT 5mm SEPARATION
PARAMETER: RADIAL DISTANCE OF PROBES TO MAIN GAP
5 cm •
10 cm ×
15 cm ○
TEMPERATURE (°K)
DELAY AFTER SPARK INITIATION (ms)

CHAPTER 5: DISCUSSION OF RESULTS

In this section some general features of the radial temperature curves are discussed and general comments about these measurements and recovery measurements are made. The derived temperatures for very short delay times are higher than one would expect, hence, a discussion of the errors involved in the measurements and in the assumption that the probe conductance is proportional to the three-halves power of the temperature.

5.1 FEATURES OF RADIAL TEMPERATURE CURVES

The curves shown in Figures 4.8 to 4.11 will be discussed in three categories and, for convenience, will be referred to as: high pressure, where the gas pressure is 10 mmHg or greater; medium pressure or 1 mmHg gas pressure; and low pressure or 0.1 mmHg gas pressure. The curves in each category are of essentially the same form.

The curves in the high pressure category all show that the gas recovers quickly and that there is little ionization present after 5 ms. Churchill (1963) reports that, using reignition techniques, he found no great variation in the recovery of the spark channel in the pressure range investigated (200 - 760 mmHg). The temperatures deduced in this experiment from probe conductance measurements confirm this in a

pressure range between 10 and 200 mmHg.

For a gas pressure of 1 mmHg the recovery was much slower. The spark channel had expanded to fill the whole spark chamber and this allowed one to to measure the radial temperature profile shown in Figure 5.1. This graph shows that for long delay times the temperature is lower close to the electrodes than it is at larger radial distances. This effect is probably due to the cooling effect of the main electrodes. The existence of detectable ionization at a radial distance of 15 cm implies that virtually the whole spark chamber is filled with plasma. This plasma is in contact with the large cold brass rods supporting the main electrodes and is cooled by them. At lower pressures, where the recovery is slower, one would then expect that the thermal cooling effect of the electrodes and their supports would be noticeable, as is the case.

In the low pressure region the temperature curves show that within the expected error (see Section 5.3) the gas throughout the spark chamber is at the same temperature. The mean free path of the particles, in this region, is of the same order of magnitude as the chamber dimensions and because of the long mean free path the gas everywhere in the chamber is at the same temperature and deionization and recovery take place at the same rate.

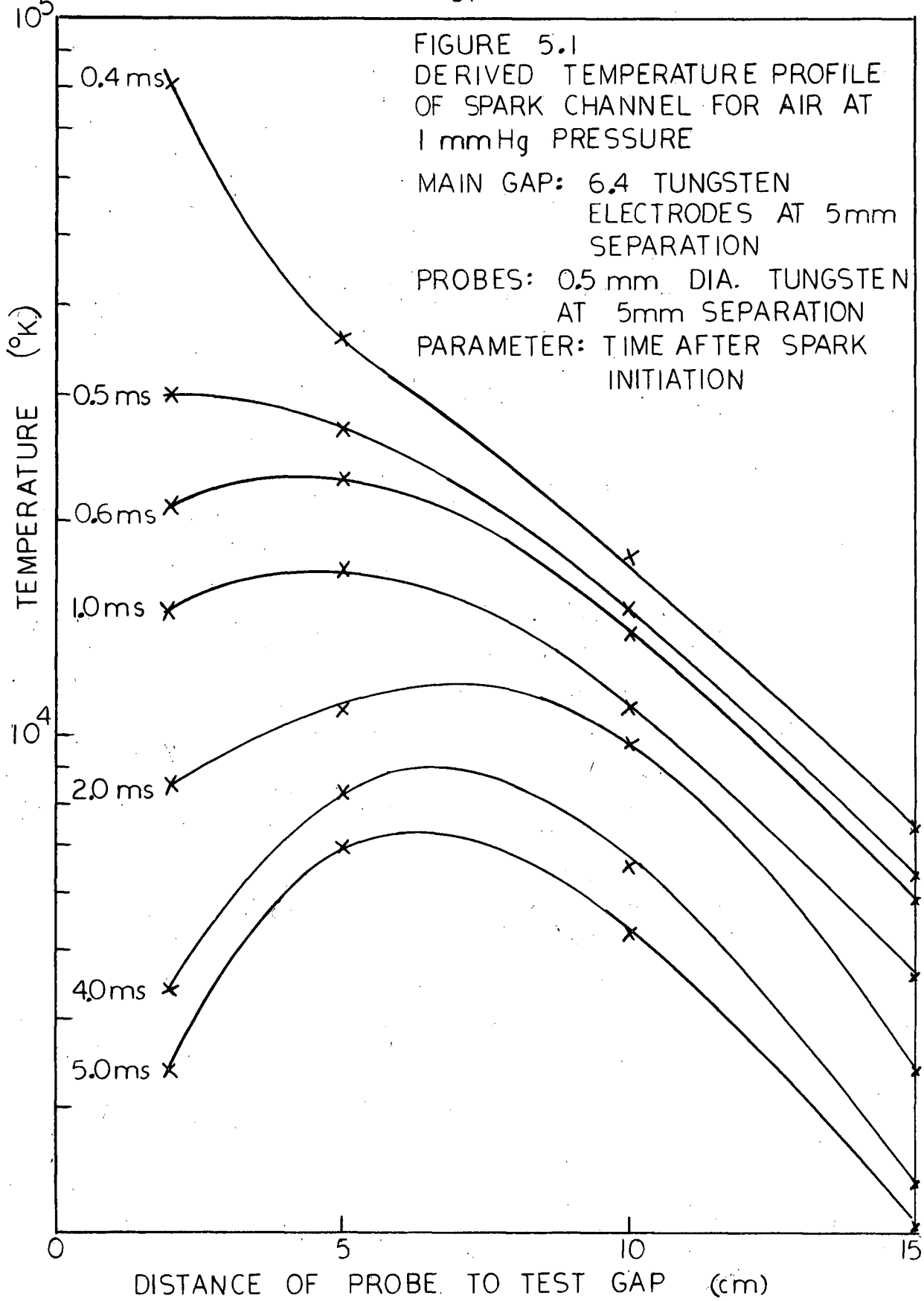
FIGURE 5.1
DERIVED TEMPERATURE PROFILE OF SPARK CHANNEL FOR AIR AT 1 mm Hg PRESSURE
MAIN GAP: 6.4 TUNGSTEN ELECTRODES AT 5mm SEPARATION
PROBES: 0.5 mm DIA. TUNGSTEN AT 5mm SEPARATION
PARAMETER: TIME AFTER SPARK INITIATION
0.4 ms
0.5 ms
0.6 ms
1.0 ms
2.0 ms
4.0 ms
5.0 ms
10^5
10^4
TEMPERATURE (°K)
0
5
10
15
DISTANCE OF PROBE TO TEST GAP (cm)

5.2 GENERAL RECOVERY CHARACTERISTICS

Assume that the region where some probe conductance is detectable is an indication of the radial extent of the spark channel. From Table III (page 43) one sees that the spark channel radius increases with decreasing gas pressure until at 1 mmHg it extends to the radial extent of the spark chamber. The temperatures which are derived from the probe conductance measurements show that the spark gap takes longer to recover at low pressures than it does at high. This observation supports the fact that the main deionization mechanism is volume recombination (see Craggs, 1963) although for complete verification the values of the electron, ion, and neutral concentrations should be known.

5.3 LIMITS OF ACCURACY OF THE RESULTS

There are a number of effects which limit the accuracy of the experimental results. As was pointed out in Chapter 3, the variation in the measured probe conductance from test to test was large and, as is to be expected, there is a large scatter in the plotted experimental points (see Figures 4.4 to 4.7). The reignition voltage calculated for the delay time of 2 ms was very close to the minimum voltage obtainable from the restriking voltage generator.

The value of the derived temperature is much higher for short delay times than one would expect, based on temperature measurements and estimates made by other workers (Craggs, 1963; Poole, Parker, and Churchill, 1963). The reason for the discrepancy is probably that the assumed constant K in equation 7 does vary due to two factors which compose this constant, $\ln\Lambda$ and the sheath thickness d. Both these factors vary with changes in temperature and particle density. Referring to the tabulated values of $\ln\Lambda$ in Spitzer (1956), one sees that for expected changes in density and temperature $\ln\Lambda$ may change by a factor of two or three. The sheath thickness is also a function of the gas temperature. Although it is difficult to estimate sheath thickness variations, they should be small, as current saturation always occurs for approximately the same applies voltage and this voltage is much in excess of $\frac{k\,T}{q_e}$.

The arguments advanced in this section imply that the derived temperature curves obtained in this experiment will accurately describe the state of the gas near the values of conductance, or temperature, for which K was calculated, with the accuracy of the derived temperature decreasing as the values of the temperature change from the calibration value. Hence low values of temperature (about 10^3 ^{o}K) are relatively accurate but the high values which occur at short (0.2 - 0.5 ms) delay times are probably in error by a factor of two or three.

However, as was shown earlier in the Chapter, a great deal of information can still be derived from these temperature curves.

CONCLUSION

From the results of this experiment it can be concluded that:

a. The conductance of two electric probes placed in a recovering spark channel, which is created by a 25 kA unidirectional current pulse, can be measured using apparatus in which the minimum measureable value of the probe conductance is about 10^{-8} mho. The following conditions must apply: the gas pressure less than or equal to 200 mmHg, the delay time greater than 0.2 ms, and the radial distance of the probes to the main gap at least 2 cm.

b. From these conductance measurements the temperature can be derived by assuming that the probe conductance is proportional to the three-halves power of the temperature. However, for delay times less than 5 ms the gas temperature is higher than one would expect from estimates and measurements by other workers (for example Craggs, 1963; Poole, Parker, and Churchill, 1963) using similar apparatus. This discrepancy is probably because the assumed constant of proportionality between the probe conductor and the temperature, in

actuality changes slowly with changes in particle density and temperature.

c. The size of the spark channel and also the time required for the channel to deionize increases with decreasing gas pressure. This implies that the dominant method of channel recovery is volume recombination.

The relative success of this experiment indicates that further probe studies should be undertaken, in which the probe conductance is measured to a higher degree of accuracy and the probe circuit gated (see Section 2.6) so that delay times less than 0.2 ms can be investigated. It is recommended that the classical floating double probe of Johnson and Malter (1950) be used to determine electron temperature and electron densities for gas pressures below 1 mmHg.

If it is possible to determine, in a detailed quantitative manner, the effect that grounding one probe has on the positive ion drift current, then the ion density can also be determined, using the drift current equation, from the data in this experiment.

REFERENCES

Allen, J.E. and Craggs, J.D., 1954. Brit. J. Appl. Phys., 5, 446.

Allan, J.W.S., Edels, H., and Whittaker, D., 1961. Proc. Phys. Soc., 78, 948.

Butter, D.A.M., 1963. M. Sc. Thesis, University of British Columbia.

Chan, P.W., 1963. M. Sc. Thesis, University of British Columbia.

Churchill, R.J., 1961. Proceedings Fifth International Conference on Ionization Phenomena in Gases, Munich 1961, (North Holland, Amsterdam, page 1075).

Churchill, R. J., 1961. Plasma Physics (J. Nuclear Energy, pt. C) 3, 291.

Churchill, R.J., 1963. Can. J. Phys., 41, 612.

Churchill, R.J., Parker, A.B. and Craggs, J.D., 1961. J. of Electr. and Contr., 11, 17.

Churchill, R. J. and Poole, D.E., 1963. Paper presented at the Sixth International Conference on Ionization Phenomena in Gases, Orsay, France, July 8-13.

Cobine, J.D., 1958. Gaseous Conductors. (Dover, New York).

Craggs, J.D., 1963. Proceedings Sixth International Conference on Ionization Phenomena in Gases, Orsay, France, July 8-13, (page 423).

Craig, R.D. and Craggs, J.D., 1953. Proc. Phys. Soc. B., 66, 500.

Delcroix, J.L., 1960. Introduction to the Theory of Ionized Gases. (Interscience, New York) pages 112-114.

Fischer, H., 1957. J. Opt. Soc. Amer., 47, 981.

Fischer, H., 1958. Proceedings of Conference on Extremely High Temperatures, New York.

Johnson, E.O. and Malter, L., 1950. Phys. Rev., 80, 58.

Loeb, L.B., 1955. Basic Processes of Gaseous Electronics. (University of California Press, Berkley).

Mc Cann, G.D. and Clark, J.J., 1943. Trans. Amer. Inst. Elec. Engrs., 62, 45.

Poole, D.E., Parker, A.B. and Churchill, R.J., 1963. J. Electrc. and Contr., 15, 131.

Rose, J.D. and Clark, M., 1961. Plasmas and Controlled Fusion. (M.I.T. Press, Cambridge, Mass.).

Smy, P.R., 1963. Can. J. Phy., 41, 1346.

Spitzer, L., 1956. Physics of Fully Ionized Gases. (Interscience, New York).

Stotz, K.C., 1963. NASA Technical Note D-2226. (Investigation of Plasma Afterglows with Application in Nitrogen).

Vanyukov, M.P., Mak, A.A. and Muratov, V.R., 1959. Optics and Spectroscopy, 6, 8.

Vanyukov, M.P., Mak, A.A. and Muratov, V.R., 1960. Optics and Spectroscopy, 8, 233.

Vanyukov, M.P., Muratov, V.R., and Mukhitdinova, I.A., 1961. Optics and Spectroscopy, 10, 294.

Clements, Reginald Montgomery, 1940-

Radical temperature derived from probe conductance measurements in a recovering spark channel. [Vancouver] The University of British Columbia, 1964.

64 l. illus., diagrs., tables. 28 cm.
Thesis(M.A.Sc. in Physics) - The University of British Columbia, 1964.
"References": leaves 63-64.

1. Electric conductivity.
2. Ionization of Gases. I. Title.

nb